

**TECHNISCHE
UNIVERSITÄT
DRESDEN**

Comparing field ionization models in simulations of laser-matter interaction

Bachelor-Arbeit
zur Erlangung des Hochschulgrades
Bachelor of Science
im Bachelor-Studiengang Physik

vorgelegt von

MARCO GARTEN
geboren am 24.09.1990 in Wolfen

Institut für Kern- und Teilchenphysik
Fachrichtung Physik
Fakultät Mathematik und Naturwissenschaften
Technische Universität Dresden
Abt. Laser-Teilchenbeschleunigung
Institut für Strahlenphysik
HZDR, Helmholtz-Zentrum Dresden Rossendorf
2013

Eingereicht am 10. Juni 2013

1. Gutachter: Prof. Dr. Thomas Cowan
2. Gutachter: Prof. Dr. Ulrich Schramm

Abstract

Field ionization plays an important role in modeling the interaction of high-power, ultra-short lasers pulses with matter. Many field ionization models exist that have predictive capability at non-relativistic laser intensities and for laser pulse durations that much longer than the atomic time scales. Most existing models take a quasi-static approach to the laser field on atomic dimensions and time scales. Yet, with pulses as short as a few ~ 10 to ~ 100 as and intensities of 10^{21} W/cm² the feasibility of these approximations becomes questionable. Still the exploration of plasma effects in relativistic laser matter interaction requires to test the boundaries of validity for these models. This thesis will take a step to point out the difficulties to be considered when existing ionization models are applied to such extreme cases.

Zusammenfassung

Feldionisation spielt eine wichtige Rolle in der Modellierung der Wechselwirkung hochintensiver, ultrakurzer Laserpulse mit Materie. Es existieren bereits zahlreiche Modelle, die akkurate Vorhersagen im Bereich nicht-relativistischer Intensitäten und oberhalb atomarer Zeitskalen treffen können. Diese begegnen dem Laser-Feld mit einem quasi-statischen Ansatz auf atomaren Längen- und Zeitskalen. Unter der Einwirkung von Laserpulsen im Bereich weniger ~ 10 bis ~ 100 as und Intensitäten von 10^{21} W/cm² ist die Anwendbarkeit der getroffenen Annahmen jedoch fragwürdig. Dessen ungeachtet ist es notwendig, die Gültigkeit der Modelle hinsichtlich relativistischer Laser-Materie-Wechselwirkung zu testen. Diese Arbeit gibt einen Einblick in die Schwierigkeiten, die bei der Anwendung existierender Ionisationsmodelle auf extreme Szenarien beachtet werden sollten.

Contents

1	Motivation	1
2	Introduction	3
3	Theory	5
3.1	Atomic units	5
3.2	Basic Characteristics	7
3.2.1	Deriving an intensity from an oscillating electric field	7
3.2.2	Ionization potential	7
3.2.3	Ionization rate	8
	Laser characteristics	8
	Atom characteristics	9
3.2.4	Ionization probability	9
3.3	Physical Ionization effects	10
3.3.1	Multi-photon Ionization	10
	Below Threshold	10
	Above-Threshold	14
3.3.2	Field Ionization	15
	Barrier Suppression	15
	Tunneling	17
3.4	Ionization Models	18
3.4.1	Landau-Lifshitz	18
3.4.2	Keldysh theory	20
3.4.3	Ammosov, Delone, Krainov (ADK)	23
3.5	Overview	26
3.5.1	Parameters, Rates and Probability	26
4	Methods	29
4.1	Guideline of approach	29
4.1.1	Spatial distribution	30
4.2	Technical implementation	31

5	Results and Interpretation	33
5.1	Ionization rate field strength dependency	33
5.2	Ionization rate Z-dependency	35
5.2.1	Analytic treatment	35
5.2.2	Numerical results	36
5.2.3	Barrier Suppression field strengths	39
5.3	Time step influence on probabilities	41
5.3.1	Double ionization	44
5.4	Influence of the pulse duration on charge states	44
5.5	Charge state evolution for different laser wavelengths	46
5.6	Initial phases in ultrashort pulses	51
5.7	Spatial charge state distribution	54
6	Conclusion	59
7	Outlook	61
7.1	Outlook	61
8	Bibliography	63

1 Motivation

Particle-in-Cell (PIC) codes are important in the simulation of laser-matter interaction. Today scientists are able to produce laser pulses of relativistic peak intensities and below-femtosecond duration. A property of such pulses are large intensity gradients both in time and space. Therefore, the question arises if existing field ionization models manage to describe the processes correctly and how the models perform in comparison to each other. In this thesis three commonly used field ionization models will be examined to look for possible problems in the application of these non-relativistic models to extreme scenarios. To point out problems to be considered in PIC simulations when the models are pushed to their limits will be the main focus of this thesis.

List of abbreviations

AU	Atomic Units
PIC	Particle-In-Cell
SE	Schrödinger equation
MPI	Multiphoton Ionization
ATI	Above Threshold Ionization
TI	Tunneling Ionization
BSI	Barrier Suppression Ionization
LOPT	Lowest-Order Perturbation-Theory
LL	Landau-Lifshitz
K	Keldysh
ADK	Ammosov-Delone-Krainov

Table 1.1: List of abbreviations.

2 Introduction

This thesis focuses on the comparison of three commonly used field ionization models. It aims to representatively point out issues in laser-matter interaction simulations for short, high intensity laser pulses. Therefore the physical effects of ionization by an electromagnetic field are briefly introduced in chapter 3. In the beginning the unit system of atomic units is introduced and the two major effects, multi-photon and field ionization, are explained. Then three commonly used models for field ionization are discussed, namely the model by Landau and Lifshitz [11], the theory of Keldysh [9] and a younger variant of the well-known ADK [2] model which was modified by Krainov [10]. After this introduction the simulation methods for evaluating these models are presented, followed by a presentation of the results and their discussion.

```
5 4 4 4 4 5 4 5 4 4 4 4 4 4 4 4 4 4 4 4 4 4 5 4 4 4 4 4 4 5 4 4 5 5 5 5 5 5 5 4
5 4 4 4 4 5 4 5 4 4 4 4 4 5 4 4 4 4 4 4 4 4 5 4 4 4 4 4 5 4 4 5 4 5 5 5 5 5 4
5 4 4 4 4 5 4 5 4 4 4 4 4 5 4 4 4 4 5 4 4 4 4 5 4 4 4 4 4 5 4 5 5 5 5 5 5 4
5 4 4 4 4 5 4 5 4 4 4 4 4 5 4 4 4 4 5 4 4 4 4 5 4 4 4 4 4 5 4 5 5 5 5 5 5 4
5 4 4 4 4 5 4 5 4 4 5 4 4 5 4 4 4 5 4 4 4 4 5 4 4 4 4 4 5 4 5 5 4 5 5 5 5 5 4
5 4 4 4 4 5 4 5 4 4 5 4 4 5 5 4 4 5 4 4 4 4 5 4 4 4 4 4 5 4 5 5 5 5 5 5 5 4
5 4 4 4 5 5 4 5 4 4 5 4 4 5 5 4 4 5 4 4 4 4 5 4 4 4 4 5 4 5 4 5 5 5 5 5 5 4
5 4 4 4 5 5 4 5 4 4 5 4 4 5 5 4 4 5 4 4 4 4 5 4 4 4 4 5 4 5 4 5 5 5 5 5 5 4
5 4 4 4 5 5 4 5 4 4 5 4 4 5 5 4 4 5 4 4 4 4 5 4 4 4 4 5 4 5 4 5 5 5 5 5 5 4
5 4 4 4 5 5 4 5 4 4 5 5 4 4 5 5 4 4 5 4 4 4 4 5 4 4 4 4 5 4 5 4 5 5 5 5 5 4
5 4 4 4 5 5 4 5 4 4 5 5 4 4 5 5 4 4 5 4 4 4 4 5 4 4 4 4 5 4 5 4 5 5 5 5 5 4
```

Figure 2.1: Extract from a text file containing charge states generated by a Monte-Carlo simulation of a laser pulse interacting with a 1D sample of particles.

The analysis is concluded by applying the models to a Monte-Carlo simulation of field ionization using a Gaussian temporal and spatial profile, showing that in fact the resulting spatio-temporal charge state distributions differ when applying the various field ionization models. Finally an outlook is given on the consequences of the presented results for plasma simulations.

3 Theory

3.1 Atomic units

Atomic units (AU) form a unit system which aims to simplify the equations describing atomic processes on their respective time-, length- or energy scale. At the same time they give a feeling for how the characteristics that are considered relate to atomic scales. They allow to assess if a process is slow or fast, a length is small or large compared to atomic dimensions. The derivation of the system is explained well in ref. [12].

From the table 3.1 it can be seen that this conversion is what is usually meant by the loose phrase " e , \hbar and m_e are set equal to unity ...".

To emphasize their usefulness, take the laser wavelength of $1\mu m$, which in AU is $1.9 \cdot 10^4$ and thus very large compared to the spatial dimension of an atom. Consequently the laser frequency of 0.0456 AU is very small compared to the electron orbital frequency in hydrogen. Thus AU can help to immediately assess which physical ionization effect is dominant in a given scenario.

1 AU of	equals	in SI units	phys. relevance
Mass	m_e	$9.1094 \cdot 10^{-31} \text{ kg}$	electron mass
Length	$\frac{\hbar^2 4\pi\epsilon_0}{e^2 m_3} = a_0$	$0.5292 \cdot 10^{-10} \text{ m}$	1st Bohr radius (H)
Time	$\frac{\hbar^3 (4\pi\epsilon_0)^2}{m_e e^4}$	$2.4189 \cdot 10^{-17} \text{ s}$	$\approx \frac{150 \text{ as}}{2\pi}$, classical e ⁻ -orbit time (H) modulo 2π
Charge	e	$1.602 \cdot 10^{-19} \text{ C}$	electron charge
Action	\hbar	$1.0546 \cdot 10^{-34} \text{ Js}$	quantum of angular momentum
Permittivity	$4\pi\epsilon_0$	$4\pi \cdot 8.8542 \cdot 10^{-12} \frac{\text{C}}{\text{Vm}}$	Coulomb constant
Energy	$\frac{m_e e^4}{\hbar^2 (4\pi\epsilon_0)^2}$	$4.3598 \cdot 10^{-19} \text{ J} = 27.21 \text{ eV}$	2 Rydberg = 2 x H ground state binding energy
Velocity	$\frac{e^2}{\hbar 4\pi\epsilon_0}$	$2.1877 \cdot 10^6 \frac{\text{m}}{\text{s}} = \alpha c$	in AU speed of light equals inverse fine structure const.
El. field	$\frac{m_e^2 e^5}{\hbar^4 (4\pi\epsilon_0)^3}$	$5.1422 \cdot 10^{11} \frac{\text{V}}{\text{m}}$	classical H barrier suppression field str.
Magn. flux density	$\frac{m_e^2 e^3}{\hbar^3 (4\pi\epsilon_0)^2}$	2.3505 T	value at center of H atom by classically orbiting electron
Intensity	$\frac{m_e^4 e^{12}}{8\pi\alpha\hbar^9 (4\pi\epsilon_0)^6}$	$3.5095 \cdot 10^{16} \frac{\text{W}}{\text{cm}^2}$	appearance intensity for H

Table 3.1: Most common AU and their physical relevance. Additionally conversion factors between atomic units and SI units have been listed.

3.2 Basic Characteristics

3.2.1 Deriving an intensity from an oscillating electric field

Although the models that are discussed in this thesis use the local field strength at the position of the atom to compute the ionization rate, it is intuitive to relate in field strength to an actual laser intensity.

The intensity of an electromagnetic wave in general is calculated from the electric field strength of the wave. In the description of this field an envelope function and a phase factor can be separated.

$$E(t) = E_{\text{env}} e^{i\Phi(t)}. \quad (3.1)$$

and the intensity is given by the absolute square of the field $|E|^2$ of the field. In the region of very short pulses the validity of this simple approximation is questionable. The condition for it to be feasible is that the oscillations of the field amplitude are fast against the change of the envelope function.

$$\frac{\Delta T_{\text{period}}}{\Delta T_{\text{pulse}}} \ll 1 \Rightarrow E(t) = E_{\text{env}} e^{i\omega_0 t} e^{i\varphi(t)} \quad (3.2)$$

Only in this case the phase factor is separable into a factor containing the constant laser frequency ω_0 and a function of the time dependent phase $\varphi(t)$. To analytically calculate the intensity of a pulse where approx. (3.2) does not hold one would have to integrate the squared absolute values of the field over time. The result is then normalized with the inverse pulse duration.

$$I = \frac{1}{T_{\text{pulse}}} \int_0^{T_{\text{pulse}}} E^*(t) \cdot E(t) dt \quad (3.3)$$

Each spatial dimension requires an additional integration. As long as the condition in eq. (3.2) holds the phase factor becomes unity. The field strengths can be set equal to effective field strengths with a prefactor of $1/\sqrt{2}$. Only when the condition is violated and the laser period is nearly as long as the pulse duration both eq. (3.1) and eq. (3.3) have to be considered and the root mean square method should no be used.

3.2.2 Ionization potential

The ionization potential plays an important role in the calculation of the ionization rates. For constant external electric fields a higher ionization potential lowers the rate. Although an analytical formula for each shell electron for each element of the PSE is too cumbersome

to develop some general assertions can be undertaken for simplified cases e.g. hydrogen-like atoms. The n -th shell energy level can either be evaluated semi-classical in the Bohr model of atoms or quantum mechanically by computing the n -th matrix element of the Hamiltonian with the solutions of the Schrödinger equation. The results in both cases are

$$\mathcal{E}_n = -\frac{e^4 m_e}{\hbar^2 (4\pi\epsilon_0)^2} \frac{Z^2}{2n^2}, \quad n = 0, 1, 2, \dots \text{ (SI units)} \quad (3.4)$$

$$= -\frac{Z^2}{2n^2} \text{ (atomic units)} \quad (3.5)$$

Here n is the principal quantum number and it can be seen that atomic units simplify the expression greatly. A Coulomb-shaped atomic binding potential was assumed in the derivation of these formulae. In reality this assumption has to be treated skeptically as the influence of every external field changes the shape of the binding potential. This change in potential can be accounted for if the Stark effect is taken into consideration [8]. It describes the removal of degeneracy and shifting of energy levels in atoms and molecules due to an external electric field. When determining the Stark shift, one has to consider whether the external field is static or alternating. More on this matter can be found in the paper of Delone and Krainov [6] where they examined the AC Stark shift in subatomic fields. They conclude that the Stark shift deepens the potential well and makes the atoms harder to ionize.

$$\delta\mathcal{E}_n(F) = \frac{F^2}{4\omega^2} \quad (3.6)$$

Delone and Krainov also predict that its influence is lowest in noble gases and largest in alkali atoms. This statement however is found to be valid only for the ground state energy level. Note that instead of writing $|\mathcal{E}_{ip}|$ because the binding energies are negative, as a convention it will be written \mathcal{E}_{ip} , thus representing a positive amount of energy to be provided for ionization.

3.2.3 Ionization rate

The ionization rate Γ describes how many ionization processes per unit time occur. The concept of an ionization rate is based on the approximation that for a limited amount of time the conditions enforcing the ionization process can be treated as constant. Since the invention of the laser multiple models have been developed to describe ionization. In the following the most important atomic and laser properties required to calculate ionization rates are introduced.

Laser characteristics

The ...

Intensity I and field strength E characterize the power of the laser pulse in time and space. Although the local field strength at the location of the atoms will be used in the calculation of the rates, for reasons of simplicity it is here regarded as equal to the laser field strength.

Photon energy ω can be either calculated from the laser wavelength or the respective wave number.

Ponderomotive potential U_p . It describes the strength of the oscillatory motion of the free electron in an external alternating electric field. The strength of the ponderomotive potential determines which physical process of ionization is prominent.

Polarization of the laser. Many recent approaches on field ionization show that there are differences in the ionization rate depending on whether linearly, circularly or elliptically polarized light is used. [5]

Atom characteristics

Ionization dynamics depend not only on the laser properties but also on the properties of the atomic species in question, such as: the ionization potential \mathcal{E}_{ip} , the atomic number Z and the principal quantum number n . Some ionization models also contain angular and magnetic quantum number of the electron [5].

3.2.4 Ionization probability

From a semi-classical point of view an electron which is ionized has to pass multiple energy levels in the atomic shell until it finally reaches the free continuum state. Ionization can therefore be treated as a sequence of stimulated processes which are opposite to spontaneous emission. As it is a rare process spontaneous emission exhibits low statistics and can be described as a Poisson process and as such follows an exponential distribution. If only two levels are considered, then the probability for a transition from a higher atomic level to a lower level is as follows:

$$P_{\text{spontaneous}} = e^{-\Gamma \Delta t} \quad (3.7)$$

In the argument of the exponential function the Greek letter Γ indicates the natural linewidth of the atomic transition. The Δt represents a time step during which the conditions of the system remain approximately the same. This expression then denotes the probability for the

spontaneous emission process, therefore the probability for excitation reads:

$$P_{\text{induced}} = 1 - e^{-\Gamma \Delta t} \quad (3.8)$$

In the course of this thesis we will consider ionization as a Poissonian process similar to atomic excitation. Following Bauer and Mulser [3] the probability for the electron to remain bound will also be assumed to be

$$P_{\text{bound}}(t) = \exp \left(- \int_0^t \Gamma[E(t')] dt' \right). \quad (3.9)$$

Here Γ should be understood as a rate for transitions from the bound to the continuum state. For discrete values of Γ and no explicit time-dependency of the rates eq. (3.9) reduces to eq. (3.7). Then the probability for the electron to leave the atom, provided in [3]

$$P_{\text{ionization}} = 1 - P_{\text{bound}} = 1 - \exp(\Gamma \Delta t). \quad (3.10)$$

will be the main formula for calculating ionization probabilities in this thesis. It should be pointed out that although this method is commonly used, it is strictly not valid in scenarios where the Coulomb field of the atom is strongly perturbed by the laser field, as the ionization is not well described by successive excitations to the continuum. In such a case a fully quantum mechanical treatment based on the S-matrix theory by Fermi [17] should be used to relate the bound state in an atom to the free continuum state of the electron. By applying this method the transition is performed in one step and the square of this transition matrix results in the ionization probability. This method does not imply the existence of an ionization rate which might be helpful if the conditions of the system vary rapidly.

3.3 Physical Ionization effects

In the following several ionization effects and the constraints on the laser pulse properties ω , \mathcal{E}_{ip} under which they are valid will be listed.

3.3.1 Multi-photon Ionization

Below Threshold

Multi-photon Ionization models the ionization process of an atom in the particle picture which means that the incoming light is treated as a flux of incoming photons. The atomic shell has several levels of energy for which the distance to one another decreases with the proximity to

condition	ionization regime
$\omega > \mathcal{E}_{\text{ip}} \gg U_{\text{p}}$	Single-photon
$\mathcal{E}_{\text{ip}} > \omega \gg U_{\text{p}}$	Multi-photon
$\mathcal{E}_{\text{ip}} > U_{\text{p}} > \omega$	Above-Threshold
$U_{\text{p}} > \mathcal{E}_{\text{ip}} > \omega$	Tunneling
$E > E_{\text{crit}}$	Barrier Suppression

Table 3.2: Different ionization effects and their regime of validity depending on laser pulse properties. The characteristics denote the photon energy ω , ionization potential \mathcal{E}_{ip} , ponderomotive potential U_{p} and the critical field strength for barrier suppression E_{crit} . The conditions are expressed in atomic units.

the free continuum state by $\frac{1}{n^2}$, n being the principal quantum number. All photons carry a fixed energy $\hbar\omega$ defined by the angular frequency of the laser wave. A particular electron which resides on its energy level in the atomic shell needs a certain amount of energy \mathcal{E}_{ip} to leave the potential well. That means that a corresponding integral number n of photons have to arrive in a *short period* of time to drive the ionization process.

$$n = \left\lfloor \frac{\mathcal{E}_{\text{ip}}}{\hbar\omega} \right\rfloor + 1 \quad (3.11)$$

For the example of a $1\mu\text{m}$ wavelength laser each photon carries an energy of 1.24 eV and thus at least 11 photons are needed to overcome the ionization potential of 13.59 eV. The particular succession of energy levels the electron passes is based on probability. Opposed to the naive imagination that the photon has to provide the exact amount of energy needed for transition, the Heisenberg uncertainty principle

$$\Delta E \Delta t = \frac{\hbar}{2} \quad (3.12)$$

leads to a non-zero width of the emission- or absorption lines of an energy state. Consequently the latter take the form of a Breit-Wigner- or Cauchy-Lorentz-distribution or, for higher temperatures, a Gaussian distribution because of thermal Doppler-broadening. [8]

Lorentz – distribution :

$$\text{schematic} \quad f(x) = \frac{1}{\pi} \frac{1}{1+x^2} \quad (3.13)$$

$$\text{here} \quad f(\omega; \Gamma, \omega_0) = \frac{1}{\pi} \frac{\frac{\Gamma}{2}}{\frac{\Gamma^2}{4} + (\omega - \omega_0)^2} \quad (3.14)$$

$$\text{FWHM :} \quad \Gamma = \frac{\hbar}{\tau} \quad (3.15)$$

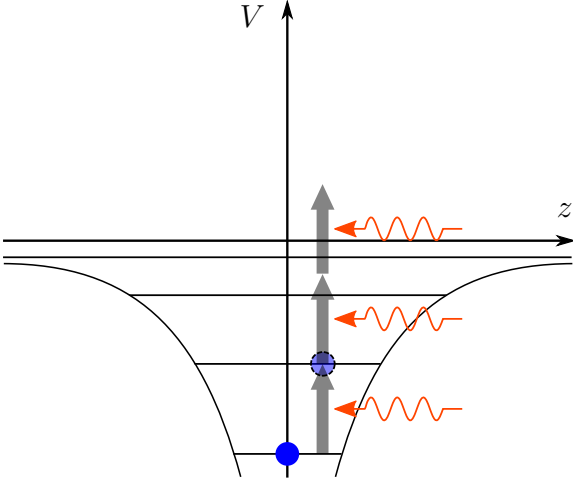


Figure 3.1: Schematic representation of the resonant multi-photon ionization. The potential shape is approximately uninfluenced by the external electric field modeled by a photon flux. In order to ionize the atoms a sufficient number of consecutive absorptions have to occur to compete with spontaneous emission. The term 'Resonant' means that an integer number of photons together match the energy of at least one absorption line of the atom.

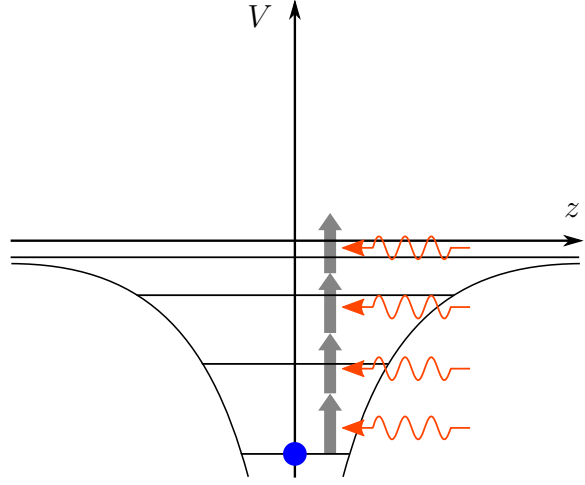


Figure 3.2: Schematic picture of non-resonant multi-photon ionization. The transition energies are not matched by the energy the incoming photons deliver. In consequence this process would result in a lower ionization rate at the same intensity than in the case of resonant MPI as the probability of exciting the transition is low.

The τ in equation (3.15) denotes the mean life time of the excited state. It gives an upper boundary for the time during which a certain number of photons must arrive to excite the electron to the next level. This non-zero width of the probability density function 3.3 shown in (3.14) makes an excitation possible even if the incoming photon delivers not exactly the energy ω_0 of the transition. The longer the life time of the excited state the narrower the transition

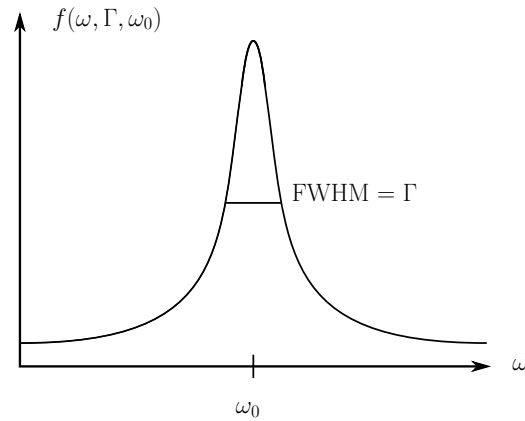


Figure 3.3: Cauchy-Lorentz distribution as a probability density function for an atomic emission line. Here, Γ denotes the natural linewidth and ω_0 the resonance frequency of the transition.

and the more improbable it becomes for the electron to be excited into this state. Multi-photon ionization can be separated into resonant and non-resonant MPI. The difference is that in the resonant process at least one transition is enhanced because the photons match its resonance frequency ω_0 . This increases the overall ionization probability. Transitions between energy levels include spontaneous and induced emission and absorption processes. In the thermal equilibrium case the transition rates are described by Einstein coefficients. In the following only the spontaneous emission coefficient A_{ji} is considered where j indicates the higher and i the lower energy state. The transition rates (here Z_{21}) for one example compute as follows:

$$Z_{21}^{(\text{spont})} = - \left(\frac{\partial n_2}{\partial t} \right)_{(\text{spont})} = A_{21} n_2 = \frac{1}{\tau_{\text{spont}}} \cdot n_2 \quad (3.16)$$

The minus sign on the right side indicates the decrease of the particle density n_2 over time. The Einstein coefficient A_{21} is the inverse of the life time for that state in regard to this special transition. The sum

$$\sum_{i < j} A_{ji} = \frac{1}{\tau_{(\text{spont})}} \quad (3.17)$$

of all Einstein spontaneous emission coefficients yield the inverse of the *total* life time of the state.

The multi-photon ionization process is complicated because it is not clear which path through the energy states the electron will take but a first estimation can be applied to locate the region of laser intensity needed. Under the assumption that the laser field strength is not altered by the Coulomb field of the atom a hydrogen atom can be approximated by a two-state-system yielding

$$\begin{aligned} I_{\min} &= \frac{n_{\text{ph}} \cdot E_{\text{ph}}}{\tau_{\text{spont}} \cdot \sigma_{\text{ion}}^{(n_{\text{ph}})}} \\ &= \frac{11 \cdot 1.24 \text{ eV}}{1.9 \cdot 10^{-7} \text{ s} \cdot 24 \cdot 10^{-24} \text{ cm}^2} \cdot 1.602 \cdot 10^{-19} \frac{\text{J}}{\text{eV}} \\ &= 4.9 \cdot 10^{11} \frac{\text{W}}{\text{cm}^2}. \end{aligned} \quad (3.18)$$

This result is obtained assuming $1 \mu\text{m}$ laser wavelength and only two levels with principal quantum numbers 1 (ground state) and 6 (quasi-ionized). The Einstein coefficients have been taken from [4] and summed up to evaluate the life time of that state. In equation (3.18) the term $\sigma_{\text{ion}}^{(n_{\text{ph}})}$ is the n -photon photo-ionization cross section taken from [21].

In the course of this thesis there have been no MPI models implemented to this point but it is being mentioned here, that in lowest-order perturbation-theory (LOPT) [7] the n -photon

ionization rate can be expressed in terms of:

$$\Gamma^{(n)} = \sigma^{(n)} I_L^n \quad (3.19)$$

Here the rate and the cross section carry the index n denoting the number of photons, while the laser intensity I is taken to the power of n as the probability of absorption for each photon is proportional to I [9]. The region of applicability for this formula is given for low field strengths E compared to the Coulomb field of the atom and high photon energies usually above the ultraviolet region of the electromagnetic spectrum (see fig. 3.8 for details). Furthermore the problem of this approach is that the sum over all possible intermediate states between bound state and continuum state is required because of the Golden Rule of Fermi which makes the process complicated to compute. The estimate given in (3.18) describes a situation where an atom would certainly be ionized. Therefore it marks the border to above threshold ionization (ATI). If the intensity would grow above this estimate then each atom would get more than the sufficient number of photons for ionization.

Above-Threshold

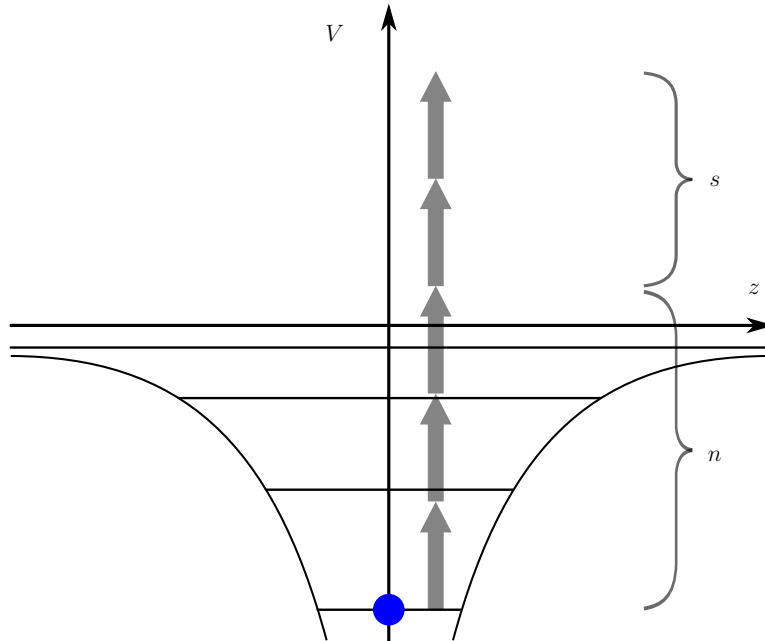


Figure 3.4: Schematic picture of the above-threshold ionization effect. At laser intensities higher than sufficient for ionization the bound electron absorbs more than the amount of photons n needed to leave the atom. The energy of the excess number s absorbed photons is converted into kinetic energy of the electron.

The main difference between the usual multi-photon ionization and above-threshold ionization is that there is an excess number of photons for each electron that is ionized and the excess

energy they deliver is converted into kinetic energy of the photo-electrons. This effect is described by Agostini et al. [1].

$$E_{\text{kin}} = (n + s)\hbar\omega \quad (3.20)$$

Here n is the number of photons needed for ionization and s is the excess number delivered.

3.3.2 Field Ionization

In contrast to MPI, field ionization treats the influence of the laser on the atom as an external electric *field*. This picture can mainly be applied for small photon energies ω compared to the ionization potential \mathcal{E}_{ip} but higher fields than in the MPI regime. It might be more intuitive to start with a classical consideration of field ionization although this approach predicts ionization at higher field strengths than a purely quantum mechanical approach.

Barrier Suppression

The classical part of field ionization is called Barrier Suppression Ionization (BSI). The atomic Coulomb potential approximated by a negative $1/r$ potential where a single electron is located in a bound state. The Hamiltonian \hat{H} of the electron, and the effective potential V_{eff} in position coordinates read:

$$\hat{H} = \frac{\hat{p}^2}{2} + \hat{V}_{\text{eff}}, \quad V_{\text{eff}} = -\frac{Z}{r} + Ez \quad (3.21)$$

Compared to the atomic potential which depends on the atomic number Z the effective potential V_{eff} depends on the external electric field E and the z -coordinate from the center of the atom.

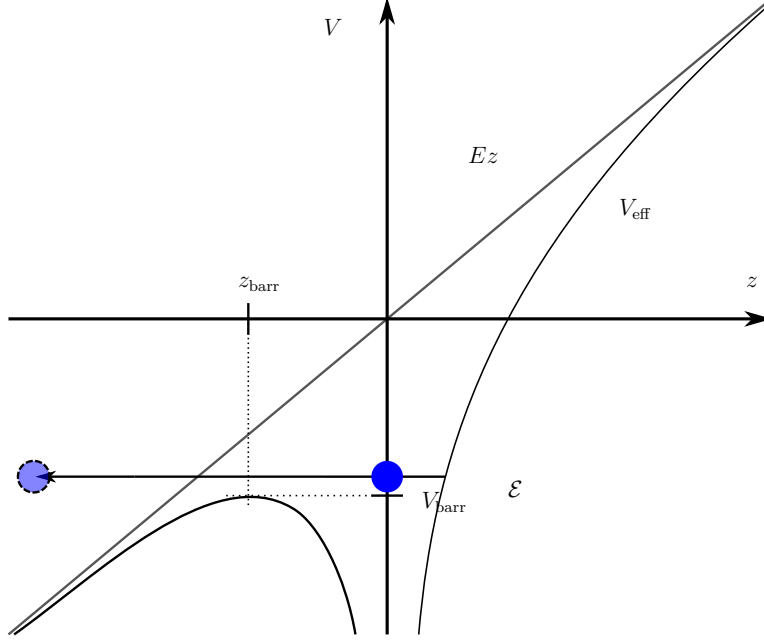


Figure 3.5: Schematic representation of the barrier suppression effect. The atomic binding potential is altered by an external electric potential Ez resulting from the quasi-static laser field strength E . The effective potential V_{eff} barrier height V_{barr} at the position z_{barr} is below the energy level \mathcal{E} of the electron. It can therefore leave the atom classically.

As shown in fig. 3.5 on the right side of the potential axis the atomic potential is modified giving an upward slope while on the other side a barrier is formed, exhibiting a maximum peak value V_{barr} . If the effective potential is derived with respect to the coordinate that peak value can be evaluated and the respective coordinate can be found. For the sake of simplicity only the z -direction of the Coulomb potential will be considered.

$$\frac{\partial}{\partial z} (V_{\text{eff}}) = \frac{\partial}{\partial z} \left(-\frac{Z}{|z|} + Ez \right) \quad (3.22)$$

$$= +\frac{Z}{z^2} + E \stackrel{!}{=} 0 \quad (3.23)$$

$$z_{\text{barr}} = -\sqrt{\frac{Z}{E}} \quad (3.24)$$

$$\text{and thus } V_{\text{barr}} = -2\sqrt{ZE} \quad (3.25)$$

In hydrogen-like atoms the energy states in AU are approximately given by:

$$\mathcal{E}_n = -\frac{Z^2}{2n^2}, \quad \text{especially for ground state : } \mathcal{E} = -\frac{Z^2}{2} \stackrel{!}{=} -2\sqrt{ZE_{\text{crit}}} \quad (3.26)$$

Here, E_{crit} denotes the critical field needed to suppress the barrier maximum to a level where it equals the atomic binding- or ionization potential. For this critical field equation (3.26)

yields:

$$E_{\text{crit}} = \frac{Z^3}{16} \quad (3.27)$$

This approximation can also be used to transform the critical field into an ‘appearance intensity’. It gives a feeling for the order of intensity a laser pulse should have to suppress the barrier

$$I_{\text{app}} = \frac{\mathcal{E}_{\text{ip}}^4}{16Z^2}. \quad (3.28)$$

The approximation assumes that the Coulomb potential of the atom remains undisturbed by the external electric field. For high intensity laser pulses the electric field strength is of the order of the atomic Coulomb field strength or even higher and the Stark shift of the atomic energy levels has to be taken into account. Bauer and Mulser derive a new critical field strength with regard to the Stark effect for hydrogen-like atoms and ions. [12]. They arrive at the result:

$$E_{\text{crit}}^{\text{H-like}} = (\sqrt{2} - 1)\mathcal{E}^{3/2} \quad (3.29)$$

This barrier suppression field strength will later on be compared to the critical field strength without considering the Stark effect and will find its application in the Monte-Carlo simulations conducted during this thesis. Due to the Stark effect the potential well is deepened and ionization rates decrease because the ionization energy is increased.

Tunneling

The concept of barrier suppression ionization does not consider the quantum mechanical behavior of the electron. It is noticeable that in V_{eff} no sharp bound states exist anymore. The reason for this is that on one side of the effective potential there is a barrier of finite height. This results in a non-zero probability for the electron to just tunnel through the barrier and leave the atom. This picture however requires the external electric field to be *quasi-static*. This is an important approximation which assumes two things. On the one hand for a sufficiently short time the external field, even if oscillating, is regarded as unchanging. On the other hand it is assumed to be spatially constant over atomic length scales. Keldysh proclaimed that the tunneling process happens with no perceptible ‘time lag’ [9], however as will later be shown in eq. (3.37) a characteristic relates to a tunneling time.

This thesis concentrates primarily on the comparison of the most commonly used ionization models and thus in the following section it is explained how each one of the models treats the tunneling process in principle to arrive at an ionization rate.

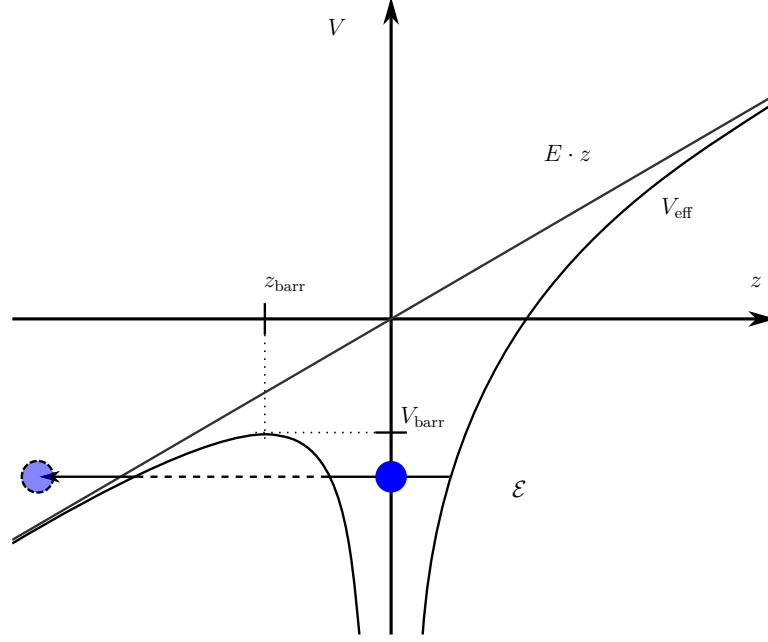


Figure 3.6: Schematic representation of the tunneling ionization effect. Requires the potential V_{eff} to be quasi-static during the process. The characteristics denote: z_{barr} position of the barrier maximum, V_{barr} the maximum barrier height and \mathcal{E} the ionization potential. The dashed line in the path of the leaving electron marks the tunneling distance.

3.4 Ionization Models

3.4.1 Landau-Lifshitz

Derivation

The Landau-Lifshitz approach for tunneling is semi-classical. At first the Schrödinger Equation is separated into parabolic coordinates (ξ, η, ϕ) by defining

$$\xi = r + z, \quad \eta = r - z \quad (3.30)$$

and gaining an effective potential. When an external field is applied to a – here hydrogen-atom – its degeneracy and symmetry is removed. The transformation in eq. (3.30) allows the decoupling into two SEs where one is for the uphill potential V_ξ and one for the downhill potential V_η .

$$V(\eta) = -\frac{1}{2} \left(\frac{1}{2\eta} + \frac{1}{4\eta^2} + \frac{1}{4}E\eta \right) \quad (3.31)$$

Then the inner potential is approximated as a quadratic oscillator potential where the ground state wave function has a non-zero width and is described by a Gaussian. Here it is assumed that the shape of the bound state wave functions are not perturbed by the effective potential.

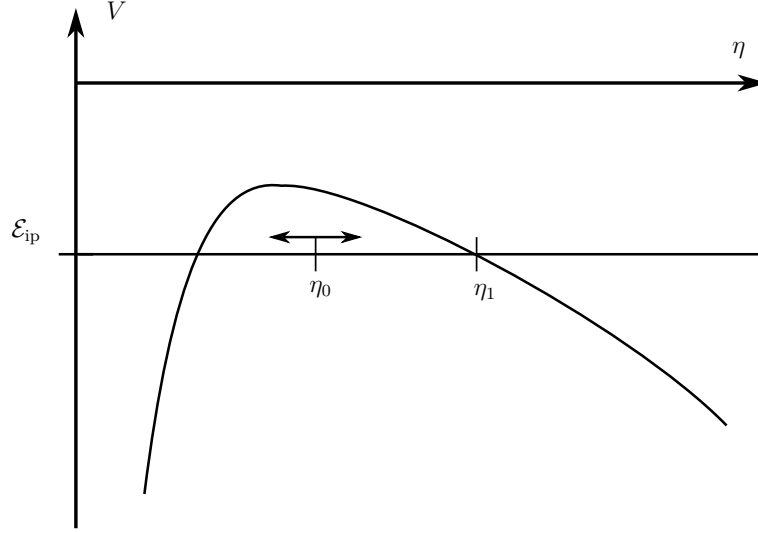


Figure 3.7: Schematic picture of the downhill potential $V(\eta)$ depicting the matching point η_0 for the tunneling wave function $\chi_{\text{left}}(\eta)$ and the electronic continuum state $\chi_{\text{right}}(\eta)$. The position η_1 shows where the electron emerges from the barrier.

The ground state energy can then be calculated as the expectation value of the Hamiltonian with the respective wave functions. The unperturbed solution of the downhill SE is multiplied with a deformation factor which depends on the electric field and leads to the critical barrier suppression field strength mentioned in eq. (3.29).

From this point on only the downhill potential V_η is considered. Landau and Lifshitz find a position inside the barrier η_0 where the boundary conditions can be matched in a similar fashion to the treatment of a one-sided finite potential well. Consequently a wave function for the left and the right side are defined:

- $\chi_{\text{left}}(\eta)$ - exponentially decreasing tunneling function
- $\chi_{\text{right}}(\eta)$ - free particle wave function

Both wave functions are semi-classical, an approximation that holds as long as the de-Broglie wavelength of the electron is small against the scale on which the potential changes. This approximation breaks again at the point η_1 where the electron emerges from the barrier because there it has no momentum and

$$p = 0 \Rightarrow \lambda_{\text{de-Broglie}} = \frac{2\pi\hbar}{p} \rightarrow \infty. \quad (3.32)$$

Landau and Lifshitz state this approach to be valid if the disagreement of the wave functions is negligible at the position η_1 . One arrives at

$$\Gamma = \frac{4}{E} e^{-2/(3E)}. \quad (3.33)$$

This is the tunneling rate for atomic hydrogen which can be easily extended to hydrogen-like ions with Z -dependency of the ground state ionization potential $\mathcal{E}_0 = -Z^2/2$:

$$\Gamma_{LL} = 4 \frac{(2|\mathcal{E}_0|)^{5/2}}{E} \exp\left(-\frac{2(2|\mathcal{E}_0|)^{3/2}}{3E}\right). \quad (3.34)$$

The integration and the assumption of a quasi-static potential set a lower limit to the time in which the model can be assumed to be reasonable. This model and all of the following *average* over the electron orbital motion.

Region of validity

- exact for low field strengths E
- overestimates ionization in over-barrier regime
- initially intended for hydrogen-like atoms and ions

Most important approximations

- wave function retains ground state shape with respect to uphill coordinate $\xi \rightarrow$ neglecting Stark shift
- de -Broglie wavelength of e^- small against potential-varying scale
- neglect disagreement between χ_{left} and χ_{right} at point where electron emerges from barrier

3.4.2 Keldysh theory

Derivation Keldysh in his publication [9] aimed to show that the nature of multi- photon ionization and tunneling ionization is essentially the same. He introduces a tunneling frequency ω_t , with

$$\omega_t = eE/\sqrt{2m_e\mathcal{E}_0} \quad (3.35)$$

and states that for low frequencies $\omega \ll \omega_t$ and strong fields tunneling ionization happens while for high frequencies $\omega \gg \omega_t$ and low fields multi-photon ionization prevails. This definition is

today widely known as the Keldysh parameter γ

$$\gamma = \frac{\omega}{\omega_t} \begin{cases} \ll 1 \rightarrow \text{tunneling ionization} \\ \gg 1 \rightarrow \text{Multi-photon ionization} \end{cases}, \quad \gamma = \omega T_{\text{tunnel}} \quad (3.36)$$

$$T_{\text{tunnel}} \simeq \int_0^{z_{\text{exit}}} \frac{dz}{|p(z)|} = \int_0^{\kappa^2/2E} \frac{dz}{\sqrt{\kappa^2 - 2Ez}} = \frac{\kappa}{E} \quad (3.37)$$

which separates the two ionization regimes from each other. The term T_{tunnel} can be interpreted

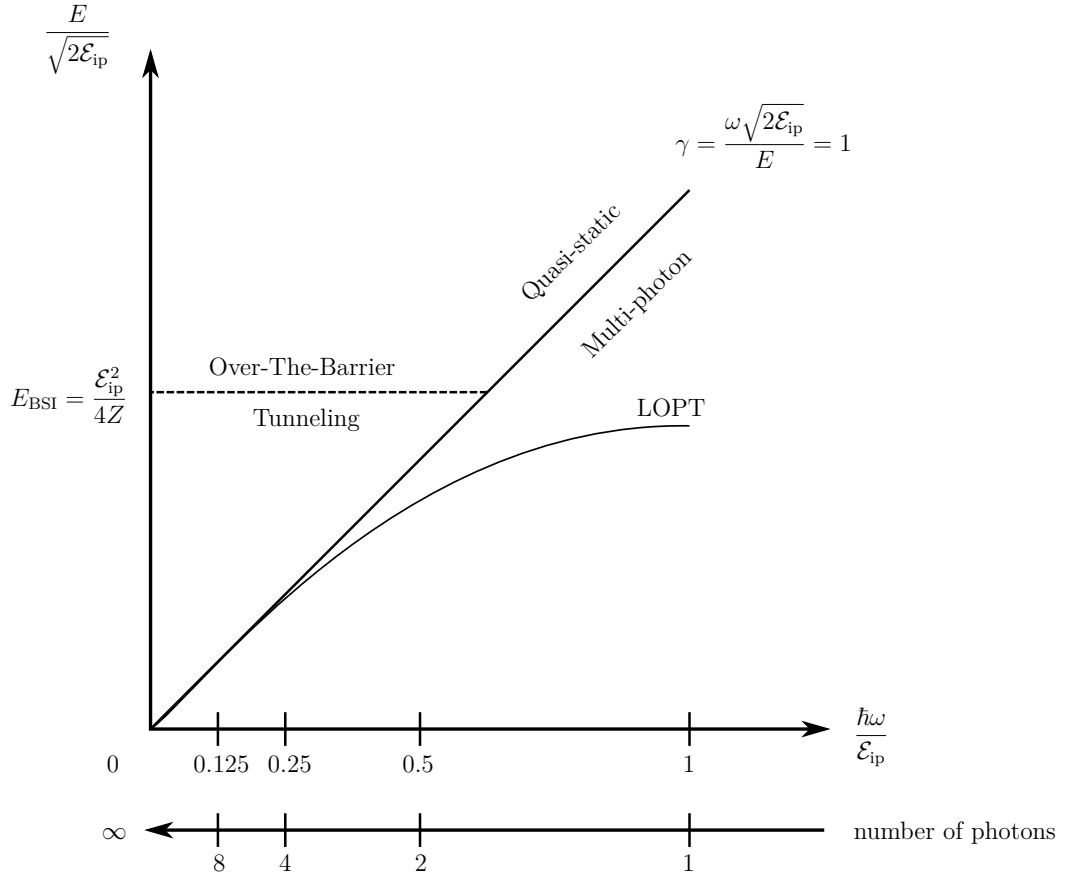


Figure 3.8: Schematic map of regions of different ionization effects in the Keldysh theory. The Keldysh parameter γ determines the boundary between field and multi-photon ionization, respectively. In the multi-photon regime the curve represents lowest order perturbation theory (LOPT) for comparison. In the quasi-static regime the barrier suppression field strength E_{BSI} separates the tunneling ionization from the over-the-barrier or barrier-suppression region.

as a "tunneling time". Eq. (3.37) yields at this result when the time to tunnel through a static Coulomb barrier is calculated in semi-classical WKB theory [16]. The parameter κ is

introduced as a characteristic momentum

$$\kappa = \sqrt{2\mathcal{E}_0} \quad \text{so that } \gamma = \frac{\omega\kappa}{E} = \sqrt{\frac{\mathcal{E}_{\text{ip}}}{2U_p}} \quad (3.38)$$

and the ponderomotive potential U_p describes the mean energy stored in the quiver motion of a free electron in an external alternating electric field.

$$U_p = \frac{E^2}{4\omega^2} \quad (3.39)$$

In his paper, Keldysh derives an ionization probability directly without considering the ionization rate. He starts with the wave functions for a free electron in an electric field and the wave function for a bound state. The probability for a transition from the latter to the former state is calculated perturbatively only with the additional assumption that the final state takes the acceleration of the free electron into account. The free electron wave function is a Volkov [20] state which considers the interaction with the external laser field whereas the influence of the Coulomb potential of the ion is neglected. The ionization probability is mainly influenced by low-momentum electronic states and thus is expanded in powers of the momentum p . In the case of low photon energies ω and large ponderomotive potentials U_p both compared to the ionization potential \mathcal{E}_{ip} the ionization probability limits in:

$$w_0 = \frac{\sqrt{6\pi}}{4} \frac{\mathcal{E}_0}{\hbar} \left(\frac{eE\hbar}{m_0^{1/2}\mathcal{E}_0^{3/2}} \right)^{1/2} \exp \left\{ -\frac{4\sqrt{2m_e}\mathcal{E}_0^{3/2}}{3e\hbar E} \left(1 - \frac{m_e\omega^2\mathcal{E}_0}{5e^2E^2} \right) \right\}. \quad (3.40)$$

In the limit of $\omega \rightarrow 0$ the second term in the exponential function vanishes. If now this probability is transformed to atomic units and divided by a unit time the same expression for the tunneling rate as in [3] is found.

$$\Gamma_K = \frac{(6\pi)^{1/2}}{2^{5/4}} \mathcal{E}_0 \left(\frac{E}{(2\mathcal{E}_0)^{3/2}} \right)^{1/2} \exp \left(-\frac{2(2\mathcal{E}_0)^{3/2}}{3E} \right). \quad (3.41)$$

A good review on the further development of the Keldysh theory has been published by Popov [14], discussing the limits of this approach.

Region of validity In the basic Keldysh theory the tunneling regime is only limited by the Keldysh parameter. Small photon energies ω compared to \mathcal{E}_{ip} and relatively large fields below the barrier suppression field strengths yield

$$\gamma = \frac{\omega\sqrt{2\mathcal{E}_0}}{E} \ll 1 \quad \Rightarrow \quad E \gg 0.0456\sqrt{2\mathcal{E}_0} \quad (3.42)$$

and in SI units for hydrogen ($\mathcal{E}_0 = 0.5$)

$$E \gg 2.34 \cdot 10^{10} \frac{\text{V}}{\text{m}} \qquad E_{\text{BSI}} = 5.1422 \cdot 10^{11} \frac{\text{V}}{\text{m}} \quad (3.43)$$

For an infrared laser of a wavelength of $1 \mu\text{m}$ the electric field strengths to which the model can be applied range between $2.3 \cdot 10^{10}$ and $5.1 \cdot 10^{11} \frac{\text{V}}{\text{m}}$.

Most important approximations

- $p(\eta_1) = 0$, only low-momentum electronic states contribute
- $\mathcal{E}_{\text{ip}} = \mathcal{E}^{(\prime)} + \frac{E^2}{4\omega^2}$, Stark effect for binding potential
- neglect influence of Coulomb potential of parent ion on final state

3.4.3 Ammosov, Delone, Krainov (ADK)

Discussion of the ionization rate On the basis of the work of Landau, Lifshitz and Keldysh multiple modifications to the obtained ionization rates have been made. Ammosov, Delone and Krainov published an ionization rate for complex atoms and atomic ions in 1986 [2].

$$\Gamma = C_{n^*l}^2 f(l, m) \mathcal{E}_0 \left(\frac{3E}{\pi(2\mathcal{E}_0)^{3/2}} \right)^{1/2} \left(\frac{2}{E} (2\mathcal{E}_0)^{3/2} \right)^{2n^* - |m| - 1} \exp \left(-\frac{2(2\mathcal{E}_0)^{3/2}}{3E} \right) \quad (3.44)$$

with

$$C_{n^*l} = \left(\frac{2e}{n^*} \right)^{n^*} (2\pi n^*)^{-1/2}, \quad (3.45)$$

$$f(l, m) = \frac{(2l+1)(l+|m|)!}{2^{|m|}|m|!(l-|m|)!}. \quad (3.46)$$

This formula introduces the effective principal quantum number n^* , the angular quantum number l and the magnetic quantum number m to the calculation. The e is the Euler-constant. The effective principal quantum number is given by

$$n^* = \frac{Z}{\sqrt{2\mathcal{E}_0}} \quad (3.47)$$

and accounts for the quantum defect in Rydberg-atoms by taking into account that the inner electrons do not entirely screen the charge of core. In review [5] it is discussed that the contribution by magnetic quantum numbers except $m = 0$ is very small and after using the Stirling formula of factorials one arrives at

$$\Gamma_{\text{ADK}} = \underbrace{\sqrt{\frac{3n^{*3}E}{\pi Z^3}}}_{\text{lin.}} \frac{ED^2}{8\pi Z} \exp\left(-\frac{2Z^3}{3n^{*3}E}\right), \quad \text{with } D = \left(\frac{4eZ^3}{En^{*4}}\right)^{n^*}. \quad (3.48)$$

The first factor in (3.48) comes from the averaging over one laser cycle and only is valid for linearly polarized light. The shape of this equation was simplified by introducing the parameter D which is often used in expressions for ionization rates and energy. The exponential term might not look familiar in this form but if n^* is resubstituted it reads

$$\exp\left(-\frac{2Z^3}{3n^{*3}E}\right) = \exp\left(-\frac{2}{3} \frac{Z^3}{Z^3} \frac{(2\mathcal{E}_0)^{3/2}}{E}\right) = \exp\left(-\frac{2}{3} \frac{(2\mathcal{E}_0)^{3/2}}{E}\right), \quad (3.49)$$

which is also to be found in eqs. (3.34) and (3.41). Physically it describes the probability density for the free electron outside the barrier which seems plausible as it converges against 1 for very high electric fields. There are yet multiple approximations to be considered here of which some are also discussed in the review [15]. Eq. (3.48) is in general valid for low fields in comparison to the barrier suppression field strength $E \ll \mathcal{E}_{ip}^2/4Z$ and the application of the Stirling formula is feasible for $n^* \gg 1$. However Delone and Krainov state that this issue poses no problem for numerical reasons.

Krainov continued the work on the ionization rate to extend its applicability into the region of barrier-suppression field strengths. In many previous approaches the free electron final state was assumed as a Volkov wave function which neglects the influence of the parent ion. In his paper [10] Krainov uses the Keldysh, Faisal, Reiss (KFR) approach which uses the S-matrix theory [17] along with a Coulomb-correction on the final Volkov state of the ejected electron. The correction factor is an exponential function with an argument that takes the same shape as the tunneling time in eq. (3.37) times Coulomb potential. It is also taken into account that the number of photons needed for ionization increases because of the Stark shift. Krainov emphasized that the pre-exponential factors enhance the ionization probability strongly. He takes the momentum distributions of the ejected electrons and integrates over them to arrive at the energy distribution for the electrons. Finally, integrating over the angles and energies he arrives at the formula for the ionization rate of atoms in the barrier-suppression regime in linearly polarized light.

$$\Gamma_{\text{BSIe}} = \frac{4\sqrt{3}}{\pi n^*} \frac{E}{(2E)^{1/3}} \left(\frac{4e\mathcal{E}_0^{3/2}}{En^*}\right)^{2n^*} \int_0^\infty \text{Ai}^2\left(x^2 + \frac{2\mathcal{E}_0}{(2E)^{3/2}}\right) x^2 dx \quad (3.50)$$

In order to compute the probability density term an integral over the square of an Airy function has to be performed. This ansatz is plausible because Airy functions are the solution to

the linear differential equation

$$\frac{\partial^2}{\partial x^2} y - xy = 0. \quad (3.51)$$

The Schrödinger equation for 1D potential wells is of the same structure and these solutions exhibit a classical turning point, which was in the derivation assumed to be inside the barrier. There, the wave function changes from an oscillatory character to an exponentially decreasing slope.

This can be seen in the asymptotic behavior of the Airy function in cases of $\text{Ai}(u \rightarrow \infty)$

$$(u \rightarrow \infty) : \text{Ai}(u) \sim \frac{e^{-\frac{2}{3}u^{3/2}}}{2\sqrt{\pi}u^{1/4}} \quad (3.52)$$

$$\stackrel{\text{resubst.}}{=} \frac{1}{2\sqrt{\pi}} \left(x^2 + \frac{2\mathcal{E}_0}{(2E)^{3/2}} \right)^{-1/4} \exp \left\{ -\frac{2}{3} \left(x^2 + \frac{2\mathcal{E}_0}{(2E)^{3/2}} \right)^{3/2} \right\} \quad (3.53)$$

$$\simeq \exp \left(-\frac{2}{3} \frac{(2\mathcal{E}_0)^{3/2}}{2E} \right) \quad (3.54)$$

If one now considers that the Airy function in the integrand is squared, the 2 in the denominator of the exponential term vanishes and it now equals the exponential term in (3.48). Note that this happens in the limit of lower field strengths where the term with E in the denominator of the Airy argument contributes strongly for small x than it would for higher fields. Higher values of x contribute only weakly, since the asymptotic behavior of the Airy function for large arguments has an exponential decrease which is more dominant than any growing power of x .

Region of validity The formula in (3.50) is intended to be applicable for both the tunneling regime $E \ll E_{\text{BSI}}$ and the barrier suppression regime $E \sim E_{\text{BSI}}$ as it can be reduced to (3.48) in the limit of smaller fields.

Most important approximations

- magnetic numbers $m \neq 0$ do not contribute
- averaged over 1 laser cycle for the linearly polarization pre-factor
- consider Coulomb correction for continuum states and Stark shift for bound states in KFR approximation [7]
- uses Stirling formula for factorials $n! \simeq \sqrt{2\pi n} \left(\frac{n}{e} \right)^n$ even for small n

3.5 Overview

In order to conclude this section the most important approximations and the regions of validity are summed up in the following two tables 3.3 and 3.4.

Model	Approximations
Landau-Lifshitz	<ul style="list-style-type: none"> - neglects Stark shift - e⁻ de-Broglie WL: $\frac{2\pi\hbar}{p} = \Delta z \Rightarrow \frac{\partial V}{\partial z} \Delta z \simeq 0$ - ignore that this breaks at position η_0 where e⁻ emerges from barrier - neglect disagreement between left- and right side wave functions at position η_1
Keldysh	<ul style="list-style-type: none"> - influence of laser field is only small perturbation - neglect Coulomb interaction of parent ion on free e⁻-state - bound states unperturbed
BSIe ADK	<ul style="list-style-type: none"> - averaged over 1 laser cycle (lin. pol.) - consider Stark shift and Coulomb correction approximately

Table 3.3: Summary of the approximations of the models

Model	ω	field strength E [AU]	intensity I [W/cm ²]
LL	$\omega \ll \mathcal{E}_{\text{ip}}$	$E < E_{\text{crit}} = Z^3/16$	$I < 2.19 \cdot 10^{15}$
K	$\frac{E}{\sqrt{2\mathcal{E}_{\text{ip}}}} \ll \omega$	$0.0456\sqrt{2\mathcal{E}_{\text{ip}}} \ll E \ll E_{\text{crit}}$	$1.6 \cdot 10^{15} \ll I < 1.5 \cdot 10^{16}$
BSIe	$\frac{E}{\sqrt{2\mathcal{E}_{\text{ip}}}} \ll \omega$	$0.0456\sqrt{2\mathcal{E}_{\text{ip}}} \ll E$	$1.6 \cdot 10^{15} \ll I$

Table 3.4: Summary of the regions of validity of the models. The column for E assumes a photon energy ω of 1 μm laser light whereas the column for I shows the value for hydrogen as an example in SI units. The characteristics denote E_{crit} - barrier suppression field strength and \mathcal{E}_{ip} - the ionization potential

Tab. 3.4 shows the general regions where the original papers assumed the models to be valid.

3.5.1 Parameters, Rates and Probability

In the following an overview about the input parameters, the ionization rates and the calculation of the ionization probability in this thesis is given.

Input Parameters

Z	atomic number
\mathcal{E}_{ip}	ionization potential
E	electric field
Δt	time step

Model Ionization rate

Landau and Lifshitz	$\Gamma_{\text{LL}} = 4 \frac{(2 \mathcal{E}_0)^{5/2}}{E} \exp\left(-\frac{2(2 \mathcal{E}_0)^{3/2}}{3E}\right)$
Keldysh	$\Gamma_{\text{K}} = \frac{(6\pi)^{1/2}}{2^{5/4}} \mathcal{E}_0 \left(\frac{E}{(2\mathcal{E}_0)^{3/2}}\right)^{1/2} \exp\left(-\frac{2(2\mathcal{E}_0)^{3/2}}{3E}\right)$
BSI-extended ADK model by Krainov	$\Gamma_{\text{BSIe}} = \frac{4\sqrt{6}}{\pi Z} \frac{\sqrt{\mathcal{E}_{\text{ip}}} E}{(2E)^{1/3}} \left(\frac{4\sqrt{2}e\mathcal{E}_0^2}{EZ}\right)^{\frac{2Z}{\sqrt{2}\mathcal{E}_{\text{ip}}}} \int_0^\infty \text{Ai}^2\left(x^2 + \frac{2\mathcal{E}_0}{(2E)^{3/2}}\right) x^2 dx$

Probability calculation

ionization probability	$P_{\text{ion}} = 1 - e^{-\Gamma \Delta t}$
---------------------------	---

Table 3.5: Overview about the input parameters, ionization rates and the probability calculation

4 Methods

This chapter focuses on the methods employed in analyzing the ionization models introduced in chapter 3 according to their dependencies on *laser* parameters and *atom* parameters.

Laser	Atomic	Results
photon energy ω	atomic number Z	ionization rates Γ
field strength E	ionization potential \mathcal{E}_{ip}	ion. probabilities P
pulse duration T_{pulse}	(quantum numbers n, l, m)	charge states Q
initial phase φ		
pulse shape		

Table 4.1: Main characteristics which can be varied in the examination of the different models

4.1 Guideline of approach

To compare the models, different combinations of the characteristics in table 4.1 have to be tested. However, for the sake of simplicity in every simulation a major number of them were kept constant.

In the following a sequence of the analyses performed in this thesis and their particular focus is shown.

Field strength dependency At first the dependency of ionization rates on static field strengths is analyzed neglecting any time-dependence of the field. The tunneling regime will be marked based on the condition $\omega \ll \mathcal{E}_{\text{ip}}$ in the case of atomic hydrogen.

Atomic number dependency Next the dependency of the ionization rate on the atomic number Z for hydrogen-like atoms is examined, assuming ionization from the ground state. Initially the models are compared in an analytic fashion, then numerical methods are used.

Extension to higher field strengths For the continuation of the models to higher field strengths a BSI condition has been chosen. The influence of the Stark shift to the barrier

suppression field strenghts is examined for the ground states of hydrogen-like ions. Afterwards the barrier suppression field strengths for Argon charge states are shown in comparison to the tunneling regime boundaries.

Ionization probabilities Different time steps are taken for the calculation of ionization probabilities from the ionization rates. They are set in context to the approximations from the model derivations. As exemplary cases a hydrogen ground state and an Ar^{4+} state are examined.

In addition the probability of double ionization will be examined in an extreme case of large electric field gradients as the following simulations only allow one ionization per time step.

Pulse dependencies The following analyses implement laser pulses of varying duration and compare the time when ionization occurs in an envelope-only case. Then the effect of an oscillating field is examined, where different wave numbers are tested for their influence on ionization dynamics. Furthermore different initial phases are employed in a short laser pulse scenario. The dependencies on wave number and initial phase are further analyzed in the course of 1D Monte-Carlo simulations.

4.1.1 Spatial distribution

The results of a Monte-Carlo simulation are shown for three distinct regions of interest in the interaction of a Gaussian-shaped pulse with a two dimensional target area. The pulse is spatially distributed and grows linearly in time during the simulation. The resulting charge state distributions are then compared to an estimate where, according to the final pulse shape, only the BSI condition is applied to the target atoms.

4.2 Technical implementation

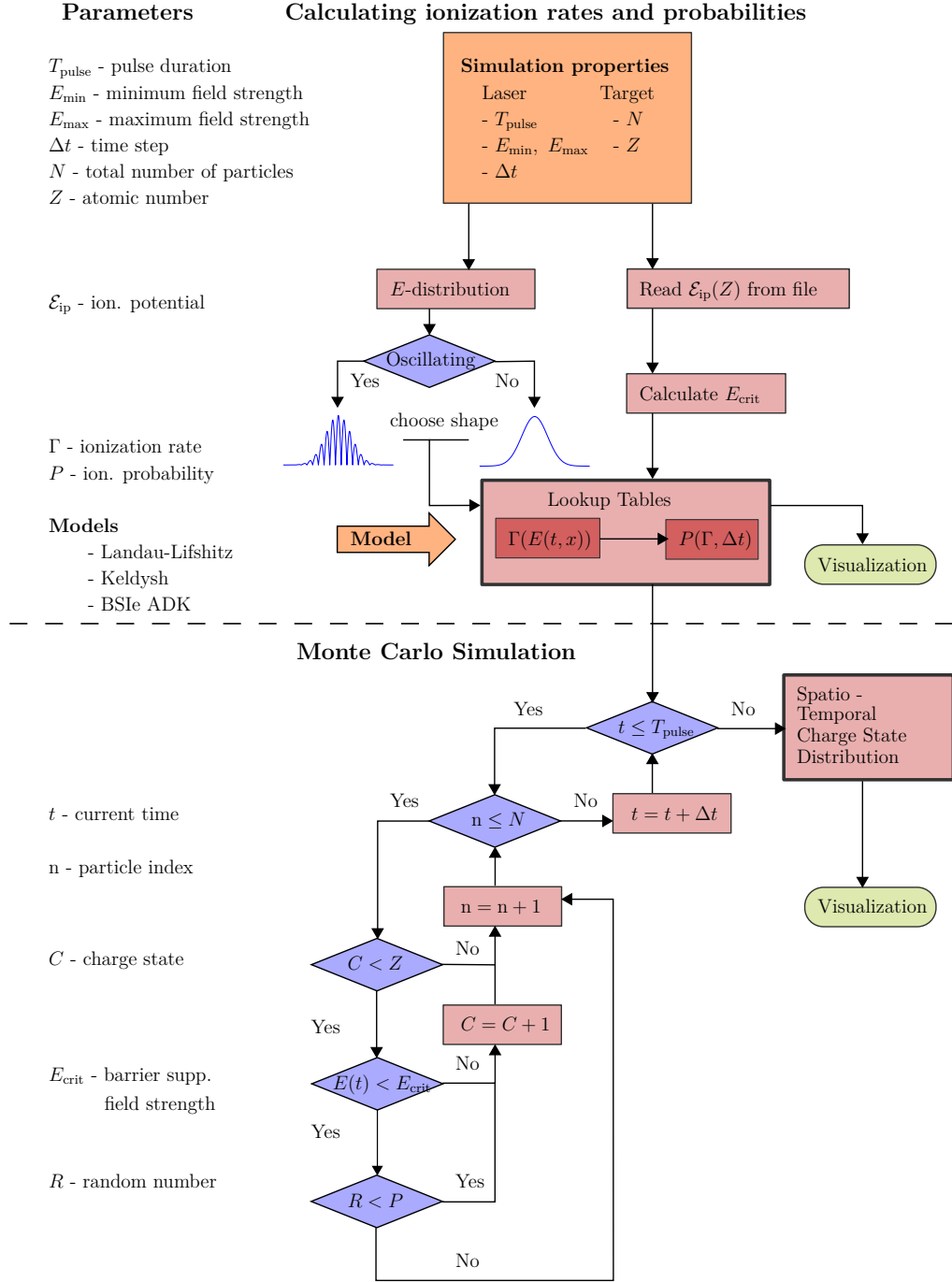


Figure 4.1: Flowchart showing the operating principles of the implementation of the ionization models into the simulations performed in this thesis.

5 Results and Interpretation

5.1 Ionization rate field strength dependency

This section focuses on a comparison of the time-independent ionization rates at different field strengths.

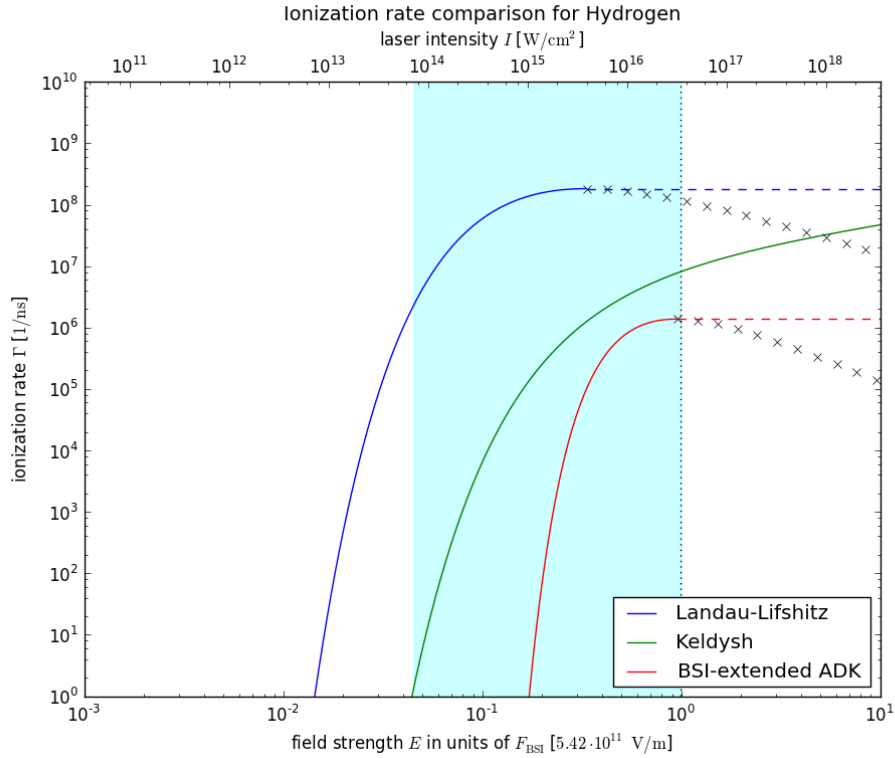


Figure 5.1: Time independent comparison of different ionization models for the hydrogen atom. The lower x-axis shows the laser field strength in units of the barrier suppression field strength of hydrogen which is equal to one atomic unit of field strength. Black crosses mark unphysical behavior and dashed lines propose a better continuation. The shaded area marks $\gamma \ll 1$ for wavelength $\lambda = 1 \mu\text{m}$

In figure 5.1 a comparison of the ionization rates for the three different field ionization models can be seen. On the lower and upper x-axis the laser field strength in atomic units and the corresponding laser intensity are depicted. In general higher values result in higher ionization rates to which the y-axis is assigned. It can be seen that the three models differ greatly as to

when the ionization rate will rise above 10^9 s^{-1} . This unit was chosen because high intensity laser pulses are generally shorter than 1 nanosecond. While the Landau-Lifshitz model starts at low field strengths of around 10^{-2} atomic units, the Keldysh model still predicts no considerable ionization rate until $4.5 \cdot 10^{-2}$ AU. Last is the BSI-extended ADK model by Krainov which starts ionizing at field strengths greater than 10^{-1} AU. Save the Keldysh model, the other two exhibit roughly the same behavior through orders of magnitude of laser intensity i.e. an initially steep slope followed by a rapid reduction of steepness at certain higher intensities. The Keldysh model ionization rate though grows not as fast as the other two and also lacks the sudden decrease in steepness seen for the other two models at field strengths close to 1 AU. The black crosses indicate where the ionization rates fall again while the field is still growing. This behavior is regarded unphysical as will be explained later. Therefore a usable continuation has been proposed which is marked by dashed lines carrying the color of the model, respectively. It assumes that the ionization rates become independent from the electric field. The cyan-colored area is the region where the Keldysh parameter γ predicts the tunneling regime for a laser of 1 micron wavelength.

Interpretation The steep slope all the models exhibit initially could result from the exponential dependence of the tunneling probability from the barrier height. For the Landau-Lifshitz and BSIe ADK model one notices that the curve for the ionization rates, including their nonphysical part, follow roughly the shape of the potential barrier in fig. 3.6. A possible interpretation for the unphysical behavior of the tunneling rates could be that with growing field strength the potential barrier is suppressed. With the suppression of the barrier, the tunneling distance diminishes. If the maximum and so the barrier suppression field strength is reached, the tunneling distance becomes zero. With further increase in the electric field there is no distance to tunnel through and the formula yields no reasonable results anymore. Consequently the rates become independent from the electric field E . It seems therefore reasonable to assume a constant rate for higher fields. The early increase of the Landau-Lifshitz rate and its unphysical behavior before the field reaches 1 AU can be explained with the neglect of the Stark shift. It underestimates the depth of the potential well of the atom. The BSIe ADK model in considering the Stark effect predicts the barrier suppression correctly at a field of 1 AU. In contrast to the other models Keldysh calculated the transition matrix elements from a bound state into a scattering state in the continuum. The model does not depend on the tunneling distance and consequently it shows no decrease of the ionization rate for growing field strengths.

5.2 Ionization rate Z -dependency

With the behavior of the models for different field-strengths pointed out, the dependency on different atomic numbers Z will be shown. An analytic treatment of the ionization rate formulae is followed by a numerical examination for the implicit field strength Z -dependency at a constant rate.

5.2.1 Analytic treatment

The previously introduced three ionization rate formulae (3.34), (3.41) and (3.48) can be simplified to examine the dependence on the atomic number Z by assuming hydrogen-like ground state ions. The latter of the three is not the BSI-extended version but the ADK rate for tunneling since it is of an easier form. Is also valid in the same regime as the other two models. All n^* and D are replaced by their original representatives and the the ionization potential reads $\mathcal{E}_{0,H\text{-like}} = Z^2/2$. Then one arrives at:

$$\Gamma_{LL}^* = Z^5 \frac{4}{E} \exp\left(-\frac{Z^5}{3E}\right) \quad (5.1)$$

$$\Gamma_K^* = Z^{5/4} \frac{\sqrt{6\pi}}{2^{9/4}} \sqrt{E} \exp\left(-\frac{Z^5}{3E}\right) \quad (5.2)$$

$$\Gamma_{ADK}^* = Z^{7/2} \sqrt{3} e^2 \left(\frac{E}{\pi}\right)^{3/2} \exp\left(-\frac{Z^5}{3E}\right) \quad (5.3)$$

In the case of small numbers Z the exponential term all of the rates have in common, can be expanded to

$$\lim_{Z \rightarrow 0} \exp\left(-\frac{Z^5}{3E}\right) = 1 - \frac{Z^5}{3E} + \mathcal{O}(Z^7). \quad (5.4)$$

The rates are then determined by their pre-exponential factors and differences between them arise. The Keldysh model assumed a $1/r$ -shaped Coulomb potential and therefore the dependence on Z is close to unity. The Landau-Lifshitz model and the BSI- extended ADK model however consider the ground state of the atom. There, the electron is under the influence of a Z/r -potential. The BSIe ADK model has an additional dependence on Z and E because it considers the Stark shift. If the field strength is smaller than 0.1 AU however the exponential term dominates and the differences between the models decrease as it converges against 0. The same behavior can be seen for field strengths up to 1 AU and large values of Z . For electric fields multiple orders of magnitude larger than 1 AU and small Z the Landau-Lifshitz model and the BSIe ADK model become unphysical as was seen before. In the case where both Z and E are large, the Coulomb fields of the atoms are strong and as such will not be suppressed

as easily by high laser field strengths. In this regime the differences are expected to be the largest due to the simple extension of the Landau-Lifshitz model and the Keldysh model to higher core charge numbers Z by inserting the measured ionization potentials. The BSIe ADK model considers the Z -dependency with the introduction of the effective principal quantum number n^* .

The Landau-Lifshitz rate decreases the least with growing Z , followed by the ADK rate and last the Keldysh rate. Yet it also has to be taken into account that while in the latter two the pre-factor increases with growing field strength E , one by the power of $3/2$ and one with $1/2$, the Landau-Lifshitz pre-factor actually drops with rising field strength by the power of -1 . The BSI-extended ADK formula, however, also exhibits such a decline-dependency in its pre-integral factors.

5.2.2 Numerical results

To account for typical targets in PIC codes and for experiments with target normal sheath acceleration (TNSA) [13] a set of atoms from different physically relevant material categories has been chosen. On every target surface there exists a thin layer of carbohydrates. Thus, we consider hydrogen, carbon and oxygen for the following analyses. From the category of gas targets the noble gas argon has been picked. Last, as representatives of condensed matter targets the lightweight element titanium and the heavier, higher Z element, gold have been added to the list. The latter is a good example since it is rarely found in an oxidized form.

Z	Symbol	Name	\mathcal{E}_0 [eV]	\mathcal{E}_0 [AU]	$ -Z^2/2 $
1	H	hydrogen	13.59	0.50	0.50
6	C	carbon	489.99	18.00	18.00
8	O	oxygen	871.41	32.03	32.00
18	Ar	argon	4426.23	162.67	162.00
22	Ti	titanium	6625.82	243.51	242.00
79	Au	gold	93254.30	3427.21	3120.50

Table 5.1: Set of atoms representing often used high-power laser experiment targets. The ionization potential for their first s-state electron is given in SI and atomic units, followed by the theoretical approximation.

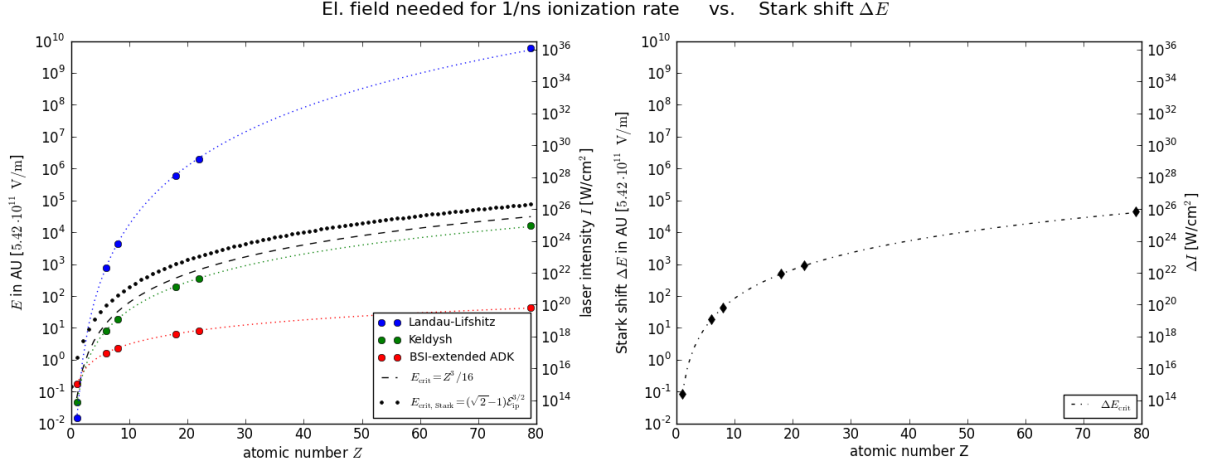


Figure 5.2: In the left plot the electrical field strengths to achieve an ionization rate of at least $1/\text{ns}$ are depicted depending on the atomic number Z . The two black dotted lines mark the barrier suppression field strengths considering (upper) and not considering the Stark shift (lower). The right plot shows the Stark shift for barrier-suppression field strengths E_{crit} of hydrogen-like states of a set of elements, containing H,C,O,Ar,Ti,Au (see tab. 5.1). The colored dotted lines for the models have been fitted by a power regression.

For these elements the ionization process stripping them off their last electron and thus resulting in a " $Z+$ "-charge state has been examined in figure 5.2 under the aspect of achieving a certain minimum ionization rate. This threshold value has been chosen to be 10^9s^{-1} . For high-power laser pulses shorter than 1 nanosecond lower rates would be of no perceivable effect in simulations. The right plot shows the Stark effect on barrier suppression field strengths E_{crit} . It is noteworthy that by shifting up E_{crit} it is nearly doubled. The left plot shows the value of E necessary to obtain the minimum ionization rate threshold. When comparing the different models it becomes obvious that only the Keldysh model follows the Z^3 -dependence from eq. (3.27). The Landau-Lifshitz model is depending on the atomic number to a higher degree and the BSI-extended ADK model yields a much lower Z -dependence as was explained before in the analytical treatment. In figure 5.2 the dependencies have been fitted according to a power regression. The three models yield

$$\text{Landau-Lifshitz : } E = 0.0137Z^{6.1032}$$

$$\text{Keldysh : } E = 0.0435Z^{2.9194}$$

$$\text{BSIe ADK : } E = 0.1694Z^{1.2611}$$

For lower Z atoms until around $Z = 3$ the roles of the three models are reversed. In the previous section it was shown in fig. 5.1 that in the Landau-Lifshitz model ionization of the hydrogen atoms was seen at much lower field strengths compared to the BSI-extended ADK model. For heavier atoms this behavior is exactly reversed as the power of Z dominates the

pre-factor.

It is noteworthy that increasing the threshold ionization rate by several orders of magnitude in the Keldysh and BSI-extended ADK model has no noticeable effect. Whereas in the Landau-Lifshitz model the field needed to reach that value increases, especially for higher- Z -elements.

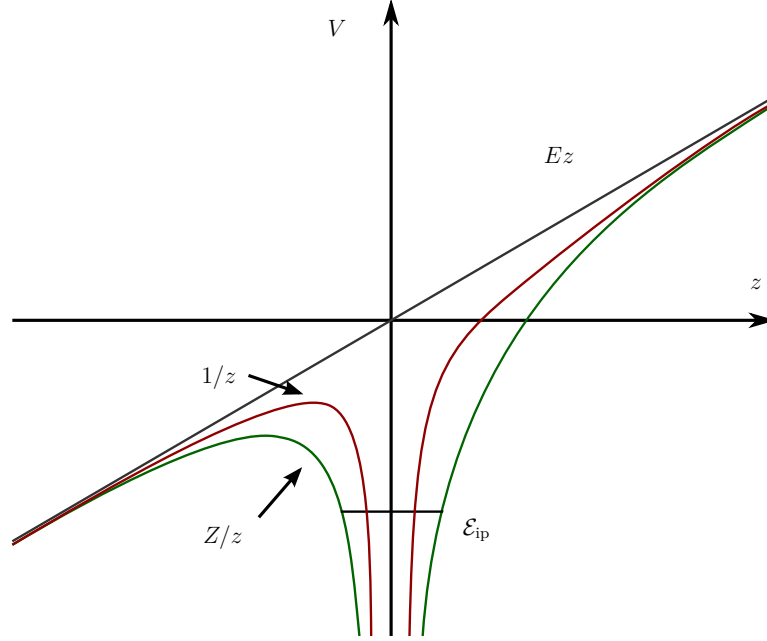


Figure 5.3: Schematic representation of an atomic potential well. The red lines depict a $1/z$ potential under the influence of an external electric field as it is assumed in the Keldysh model. The green lines depict the field-affected Z/z potential used in the derivation of the Landau-Lifshitz and the BSIe ADK model. Here, $Z > 1$ is assumed.

In figure 5.3 it becomes obvious that the Keldysh model overestimates the height of the barrier by assuming an $1/z$ potential while the other two approximate the ground state with higher accuracy.

Interpretation It was predicted by Landau and Lifshitz that for E_{crit} -near field strengths the ionization model would overestimate the ionization rates. This seems to be true for hydrogen only. It has become clear now that if an extension to other atoms by just implementing their respective ionization energies is done, the exact opposite happens for higher atomic numbers Z . The ionization rates are underestimated to an extent that they do not provide any contribution whatsoever to the ionization process if a barrier suppression condition would be introduced. This is still the case if that critical field considers the Stark shift of ionization energies. Thus, the Landau-Lifshitz model does not seem to be a reasonable choice for modeling laser-matter interaction with atomic species any other than hydrogen. The Keldysh model and the BSI-extended ADK model yield no problems in that regard. The difference between these models

however is already strong for atoms of a larger core charge than carbon. As the models were tested here only under static-field circumstances in a time- dependent simulation these differences could lead to essentially different outcomes. Furthermore it can already be predicted that, depending on the model, currently available peak laser intensities of 10^{21} W/cm² might not manage to fully ionize atoms heavier than Argon.

5.2.3 Barrier Suppression field strengths

In later parts of this chapter Monte-Carlo simulations will be analyzed. It has become obvious in the analysis of the field strength dependency that a treatment of barrier suppression ionization is necessary. In comparison to the former figure 5.2 now the corresponding barrier suppression field strengths for the example of Argon atoms are shown in 5.4. Here the critical field strengths

$$E_{\text{crit}} = \frac{\mathcal{E}_{\text{ip}}^2}{4Z} \quad (5.5)$$

$$E_{\text{crit, Stark}} = (\sqrt{2} - 1)\mathcal{E}^{3/2} \quad (5.6)$$

from eq. (3.29) have been calculated for all charge states. They are compared assuming the Stark-shifted critical field strengths mark the upper limit of the tunneling regime.

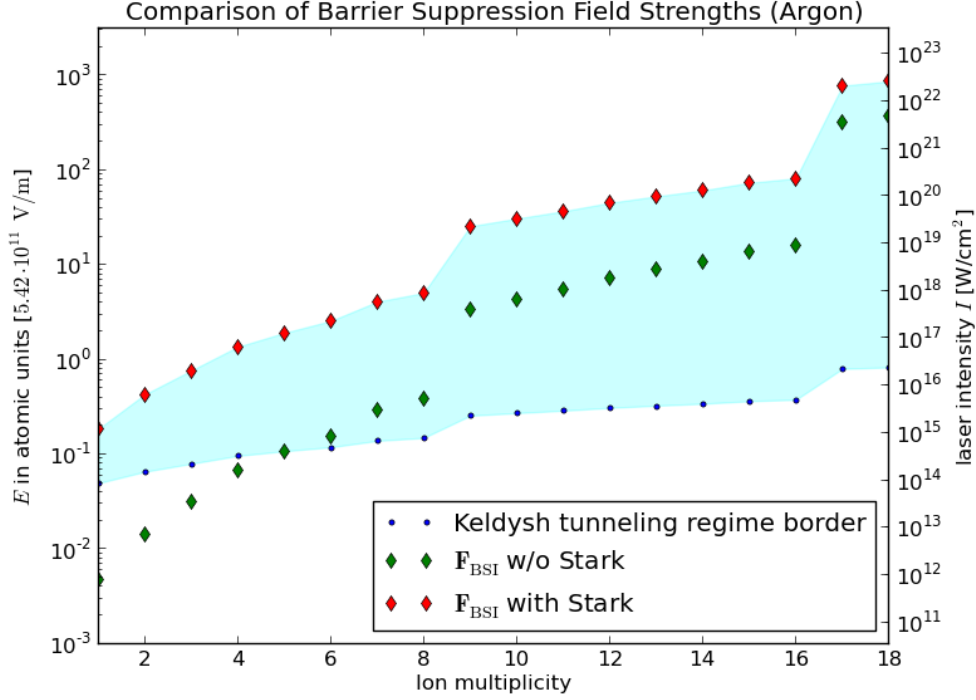


Figure 5.4: Barrier Suppression field strengths for each ion multiplicity with and without the Stark shift. The shaded area marks the tunneling regime defined by the Keldysh parameter. A laser wavelength of $1\ \mu\text{m}$ has been assumed to calculate its lower boundary for each charge state. Below the border the multi-photon regime is located.

The tunneling regime which is marked in fig. 5.4 was derived as follows

$$\lambda = 1\ \mu\text{m} \quad \Rightarrow \quad \omega = 0.0456\ \text{AU} \quad (5.7)$$

$$\gamma \ll 1 \quad \Rightarrow \quad E \gg \omega \sqrt{2\mathcal{E}_{\text{ip}}} = 0.0456 \sqrt{2\mathcal{E}_{\text{ip}}} \quad (5.8)$$

Here, \mathcal{E}_{ip} accounts for the ionization potential of each Argon charge state, thus yielding its own lower boundary for the tunneling regime. The shaded region starts where the threshold from the upper equation is located, since the condition to the Keldysh parameter $\gamma \ll 1$ is often interpreted as $\gamma < 1$. The figure shows that for growing ion multiplicity also the region for tunneling grows. If the Stark shift is not being considered, however, the first charge states lie outside the tunneling regime. Another eye-catching feature are the jumps of E_{crit} for the transitions from $8+$ to $9+$ and from $16+$ to $17+$. Those are no effect of the model but simply of the ionization energies of the Argon atom. When the first 8 electrons are removed, the noble gas Argon arrives at the noble gas configuration of Neon which is more stable. The same accounts for the jump between 16 and 17 where the completely filled s-state of the Helium configuration shows its stability.

Interpretation The barrier suppression field strengths in this thesis depend purely on the ionization potential. Therefore they depend on the atomic number Z only implicitly. For higher Z the first ionization energy of the outermost electron is still similar to hydrogen in orders of magnitude. The reason is that all inner electrons shield the core charge to some extent. As the ionization potential grows with the number of unpopulated energy levels, so does the tunneling regime with regard to the range in intensity. The calculation of the Stark-shifted barrier suppression field strengths $E_{\text{crit, Stark}}$ however was initially derived for hydrogen-like ions. Thus, a possible explanation is that the formula was applied to Argon atoms. In the application of the models for PIC codes multiple orders of magnitude of the electric field strengths are passed and different species are ionized. With such small borders it proves hard not to violate the borders of validity. If the gradients of the electric field strengths cannot be sampled to sufficient detail anymore a BSI condition has to be employed to prevent some of the models from yielding unphysical results.

5.3 Time step influence on probabilities

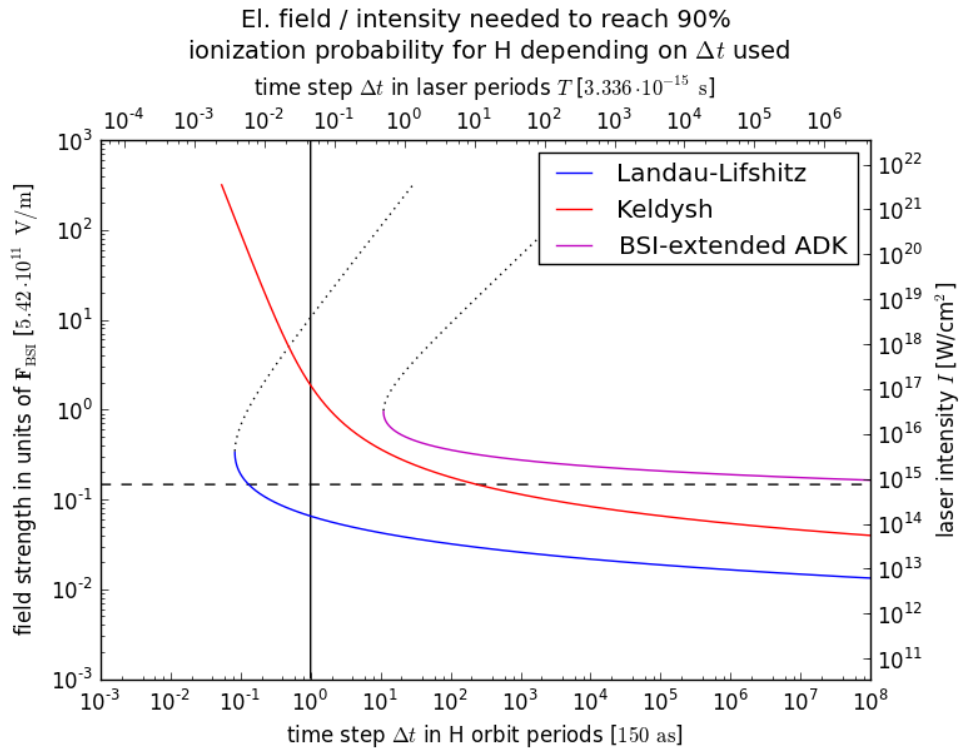


Figure 5.5: Influence of the chosen time step for computing ionization probability in several models. Different Δt result in different local field strengths / laser intensities needed to reach 90% ionization probability. The dotted black continuation of the graphs are the unphysical regions.

To emphasize the influence of the time step which in PIC simulations is generally chosen with

respect to the electron density of the material, figure 5.5 now assumes that all models are supposed to reach 90% of ionization probability. The probability is computed as discussed in eq. (3.10) in chapter 3.

$$P = 1 - \exp(-\Gamma(E)\Delta t) \quad (5.9)$$

Different time steps are used and the electric field strengths (in AU) required to reach 90% ionization probability are plotted accordingly. On the right side y-axis the corresponding laser intensity in W/cm^2 is shown. The lower x-axis shows the time step in units of one classical orbital period of the electron in hydrogen and the upper x-scale shows the time step in units of the laser period for $\lambda = 1 \mu\text{m}$, respectively.

Time steps left of the vertical black line represent time scales where the electron motion and its position have to be taken into account. The figure shows that in this region the models differ greatly. Given the time step is small enough the Keldysh model requires laser intensities outside the bounds of current capabilities. It is however the only model not in need of a continuation to higher field strengths. The Landau-Lifshitz model and the BSIe ADK model reach above 90% ionization probability in times comparable to one laser period well below the relativistic intensity of $I = 1.38 \cdot 10^{18} \text{ W}/\text{cm}^2$ for $\lambda = 1 \mu\text{m}$. The dashed horizontal line in fig. 5.5 marks the barrier suppression field strength calculated with eq. (3.29). In a simulation where a BSI condition at this field strength of about 0.147 AU would be applied, the BSIe ADK model could not ionize the hydrogen atom before the BSI condition would take effect.

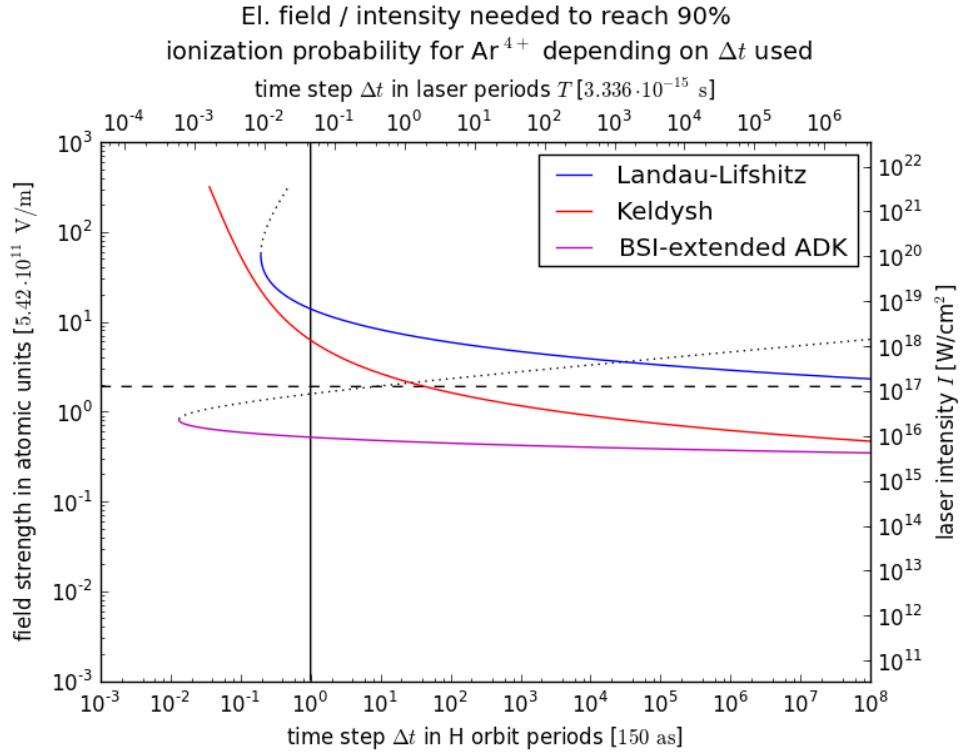


Figure 5.6: Again the influence of the time step but now on the process of ionizing Ar^{4+} . The dashed horizontal line displays the barrier suppression field strength of Ar^{4+} in AU, calculated with eq. (3.29). The dotted black continuations show the unphysical regions.

As expected, for Argon ions in fig. 5.6 the role of the models is reversed. Here, it is possible to choose a time step of a few attoseconds in every model. As can be clearly seen, the laser intensities needed to ionize Ar^{4+} differ by multiple orders or magnitude in this regime. In this example the Keldysh model is prevented from taking effect for time steps smaller than 1 laser period if a barrier suppression condition (the dashed horizontal line) is taken into account. The Landau-Lifshitz model fails to ionize the Ar^{4+} ions on time scales relevant in simulations employing the BSI condition.

Interpretation For a reasonable compromise of using the models for simulations with very short time steps there has to be a continuation of the models to larger field strengths. Choosing a time step smaller than the classical orbital period of an electron is by itself already a violation of the quasi-static assumption which was used to derive the models. If the characteristic $\Gamma\Delta t$ is small against 1 then the eq. (3.10) expands to

$$P = 1 - e^{-\Gamma\Delta t} \stackrel{\Gamma\Delta t \rightarrow 0}{\approx} \Gamma\Delta t. \quad (5.10)$$

This is now a linear dependency of the probability on the rate and the time step. Yet this is only applicable if the ionization rate is continued reasonably, which has been accounted for in this thesis by introducing the BSI condition. However it has become clear the time step has an influence on the field strengths E required for ionization and the ionization model should be chosen with respect to the atomic species. It is questionable if the concept of an ionization rate is reasonable for time steps below 1 electron orbital cycle.

5.3.1 Double ionization

Double ionization can be neglected for small time steps Δt . The probability for double ionization in all calculations performed in this thesis never exceeded more than a few percent.

5.4 Influence of the pulse duration on charge states

When keeping the same pulse shape but choosing different pulse durations it is expected that also the charge states will come to life after longer or shorter times. Previous considerations about the importance of the time step should be kept in mind when from now on it will be fixed to 1/50th of the laser period to sample the oscillating laser field at sufficient resolution. Argon is used as a target atom to yield physical ionization rates even at such small time steps.

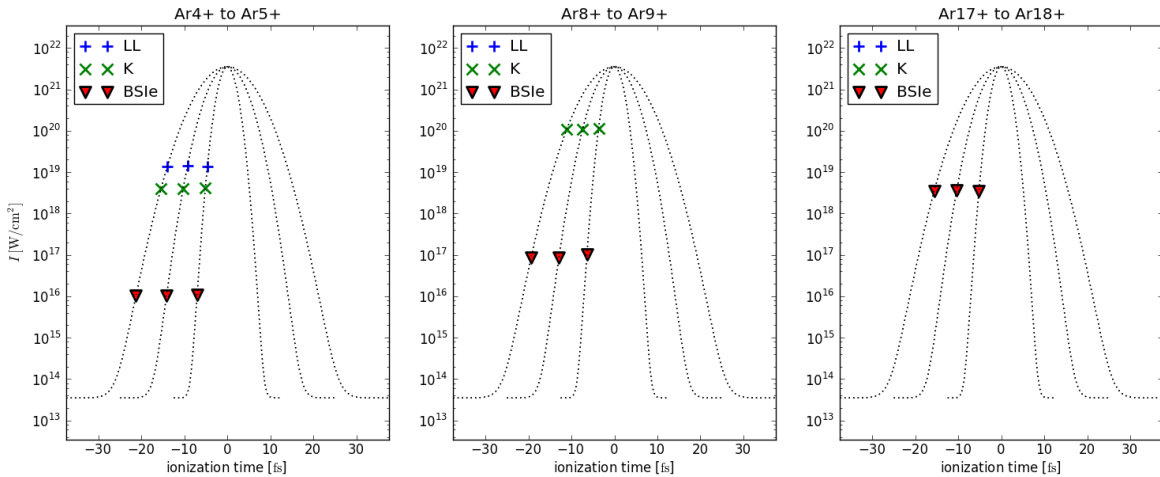


Figure 5.7: Influence of the pulse duration T_{pulse} on the emersion of charge states in Argon atoms. Three transitions are examined for their time of appearance in the three different models due to three pulses of 25, 50, 75 fs duration, respectively. The corresponding laser intensity is depicted on the y-axis. Ionization times are shown relative to the pulse maximum.

For the computation of the ionization rates and probabilities a temporal Gaussian pulse shape was used with intensities ranging from about $3.5 \cdot 10^{13}$ to $3.5 \cdot 10^{21} \text{ W/cm}^2$. Three different

pulse durations, 25, 50 and 75 femtoseconds, have been applied while the same Gaussian shape was kept. In this examination the time is extracted where the ionization probability surpasses 90 %. Since no barrier suppression condition has been applied, yet, the results are completely model-dependent. As expected the results in figure 5.7 show that first of all lower charge states emerge earlier than higher ones. Secondly, higher pulse durations account for later emersion of the same charge state. From the previous findings it could also be expected that limiting the intensity to a certain value could have the effect that in the Landau-Lifshitz model Argon's highest charge state might not be reached. This is exactly the case in the rightmost plot of figure 5.8 where only the BSI-extended ADK model manages to produce Ar^{18+} and the Landau-Lifshitz and the Keldysh model both do not predict ionization for this state. The BSI-extended ADK model depends only weakly on the scaling of the ionization potential i_p in the different charge states.

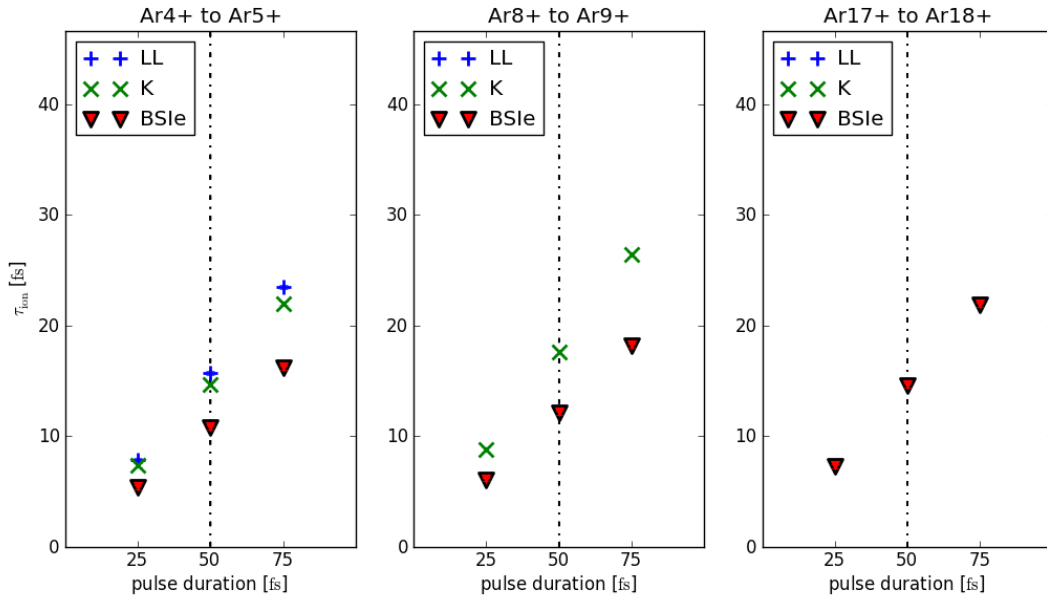


Figure 5.8: Influence of the pulse duration T_{pulse} on the emersion of charge states in Argon atoms. Three transitions are examined for their time of appearance in the three different models due to three pulses of 25, 50, 75 fs duration, respectively. The ionization times are shown in total. The pulses each reach the peak at half of the pulse duration, respectively.

In fig. 5.8 the results from fig. 5.7 are presented in a different manner, depicting the total time until ionization is reached as a function of pulse duration T_{pulse} . The dash-dotted lines indicate the pulse duration of 50 fs.

Interpretation The tests showed the simple result that for longer or shorter pulses of the same shape, there is a linear correlation between the pulse duration and the time a certain

ionization probability is reached. With regard to PIC simulations where energy conservation is not neglected pulse durations as short as the period of a laser cycle should be treated carefully. In such a case it is strictly not valid to relate the power of the pulse to a pulse with an oscillating field amplitude. For $\lambda = 1 \mu\text{m}$ the critical regime of pulse durations is located below 10 fs since a laser period T_{period} measures 3,3 fs.

5.5 Charge state evolution for different laser wavelengths

In this section the approximation of a slowly varying laser-envelope will be replaced by an oscillating electric field. In the following it will be examined if the implementation of a varying field amplitude can result in a different evolution of the charge states. Similar to 5.4 the times when 90% ionization probability occurs have been computed. In table 5.2 the set of wavelengths for the test is shown. The pulse duration is set to 50 fs which equals about 2067 AU. For the intensity of the pulses to be approximately the same, the condition $T_{\text{period}} \ll T_{\text{pulse}}$ has to be valid, as was discussed in the Theory chapter 3. Therefore the ratio of the period to the pulse duration is shown in table 5.2.

wavelength [nm]	wave number [cm^{-1}]	period [AU]	period [fs]	$T_{\text{period}}/T_{\text{pulse}}$
160	$6.25 \cdot 10^4$	22.06	0.53	0.01
320	$3.13 \cdot 10^4$	44.13	1.07	0.02
640	$1.56 \cdot 10^4$	88.25	2.13	0.04
1280	$7.81 \cdot 10^3$	176.50	4.27	0.09
2560	$3.90 \cdot 10^3$	353.00	8.54	0.17

Table 5.2: Set of wave numbers for the charge state time distribution test. In the last column the ratio between the period T_{period} and the pulse duration T_{pulse} is shown to emphasize the negligibility of the oscillation for the pulse power.

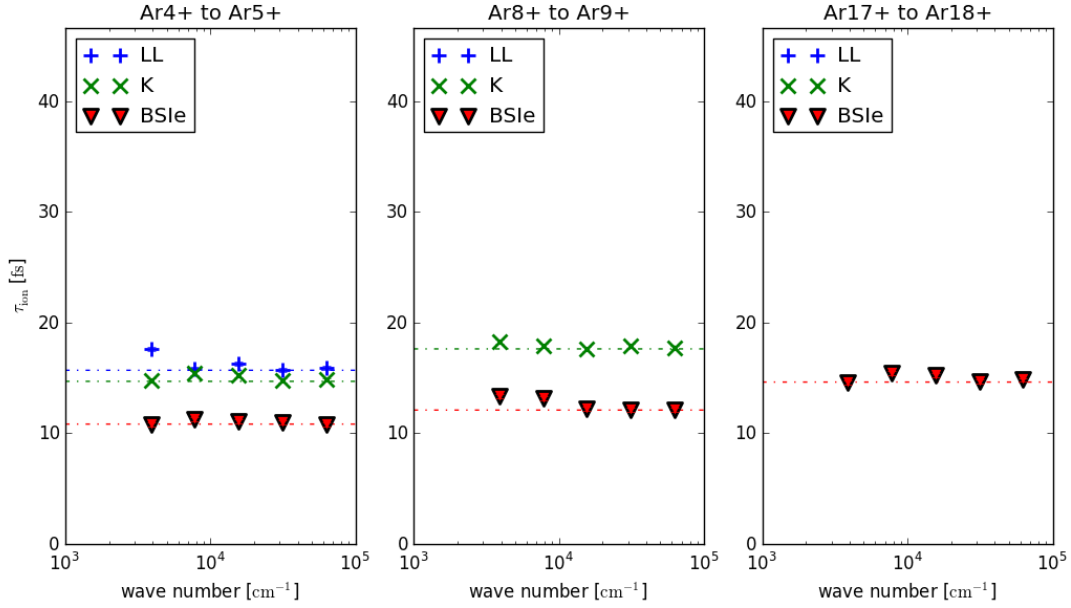


Figure 5.9: Influence of different wave numbers on the emersion of charge states in Argon atoms. The set of 5 wave numbers from tab. 5.2 determines the oscillation of electric field. The wave numbers range from about $4 \cdot 10^4$ to $6 \cdot 10^5 \text{ cm}^{-1}$. A pulse duration of 50 fs was simulated in each case and the horizontal lines indicate the results from fig. 5.8 with the slowly varying field envelope.

In comparison to figure 5.8 the implementation of an oscillating electric field into a 50 fs Gaussian pulse in figure 5.9 does not seem to affect the final states of the ions in each model. Again the Landau- Lifshitz model ionizes only the 4+-state, while the Keldysh model manages to ionize the +8-state and only the BSI-extended ADK model predicts an 18+ charge state. The colored dash-dotted lines in the figure denote the time until the ionization probabilities reach 90% as they were achieved in the analysis in section 5.4. All three plots have in common that the moment when the threshold value is reached is either the same with 5.8 or generally later. One also notices that there is no general tendency for the deviation from the envelope case that could be matched to the scaling of the wave number. It is only to be noted that if a marker deviates from the horizontal line, the deviation itself is larger for lower wave numbers. The largest deviation observed is about 4 fs.

To anticipate the interpretation of the results there ought to be pointed out that the oscillating field is very sensitive on the time step when the regions of very small pulse durations are explored. The oscillation forces the electric field to pass through multiple orders of magnitude in much shorter times than it would have before with a slowly-varying field envelope. It has become clear by now that some ionization models can exhibit only a very small region where ionization happens in a physical sense and with perceptible ionization rates. If the sampling of the laser period T_{period} is too coarse then discrete values of the electric field E might not fall into the small regime where the ionization model predicts tunneling. In comparison to the

envelope-case threshold probabilities, like $P = 90\%$ are reached with delay. Assume that the laser period is sampled well enough to contain the threshold value at some point, the delay time t_{Delay} can be quantified. If, in the worst case, the amplitude of E decreases right before the threshold value was to be reached, the threshold is exceeded not until nearly half a period has passed. This is valid if only the absolute value of the electric field is considered in the models. Lower threshold probabilities than 90% decrease the delay time.

To prevent sampling problems in the following simulations the barrier suppression conditions from (3.29) were being applied in the process. The model of Landau and Lifshitz will not be examined anymore from here on, since the barrier suppression condition forestalls the action of it. The model predicts ionization only for much higher field strengths than E_{crit}

Monte-Carlo simulations In figures 5.10 to 5.14 Monte-Carlo simulations have been used to model the interaction of a 50 fs laser pulse with Argon atoms in the cases of three laser wave numbers in the Keldysh model. The method of operation is accounted for by the flowchart 4.1. The wave numbers k in question are $3.9 \cdot 10^3$, $1.60 \cdot 10^4$ and $6.25 \cdot 10^4 \text{ cm}^{-1}$ from table 5.2. In the upper part of the figures the pulse envelope and the corresponding oscillating field is shown. The lower part depicts the evolution of charge states. The population of every charge state is indicated by the color it carries. Dark blue means the state is completely unpopulated while dark red denotes that 100% of the $N = 1000$ particles that were simulated share the charge state.

The final states are the same regardless of the wave number. Moving to larger wavelengths steepens the gradient of the field strength in time resulting in more immediate transitions between the charge states. The longer the period, the shallower the gradient of the electric field implicating that more widespread charge state distributions are possible. However as the amplitude $E(t)$ cycles through a minimum again, the meanwhile change of the envelope is larger compared to the small-period case. This results in a yet steeper field gradient at the beginning of a new laser cycle, thus enhancing the eventuality that the barrier-suppression condition instead of the model itself is doing the ionization.

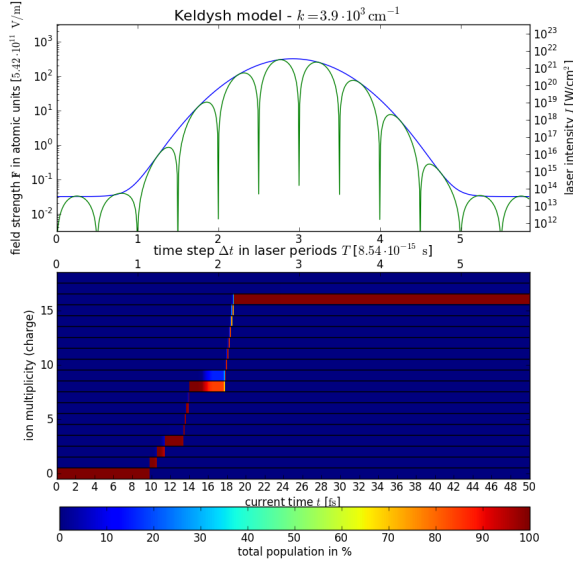


Figure 5.10: Keldysh model
Wavelength: 2650 nm, pulse duration: 50 fs

Charge state evolution for 1000 particles in a Monte-Carlo simulation. ...

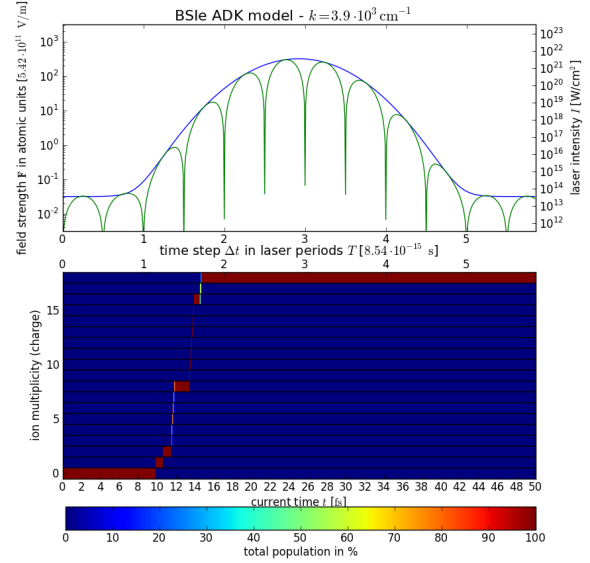


Figure 5.11: BSle ADK model
Wavelength: 2650 nm, pulse duration: 50 fs

... The green line in the upper plot marks the field strength at each moment, ...

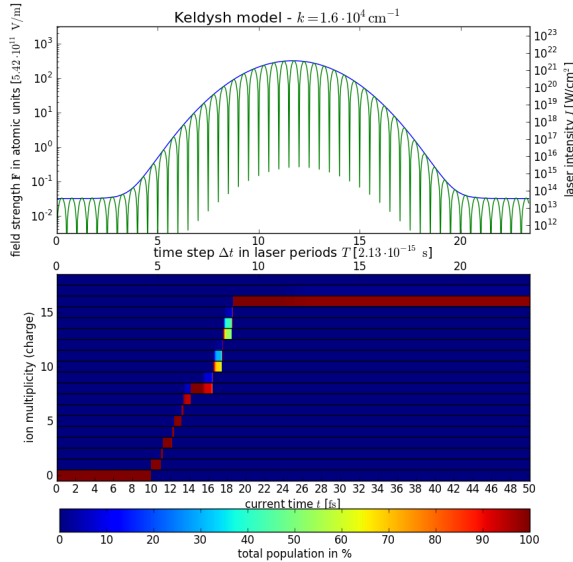


Figure 5.12: Keldysh model
Wavelength: 640 nm, pulse duration: 50 fs

... from which ionization probabilities were calculated. ...

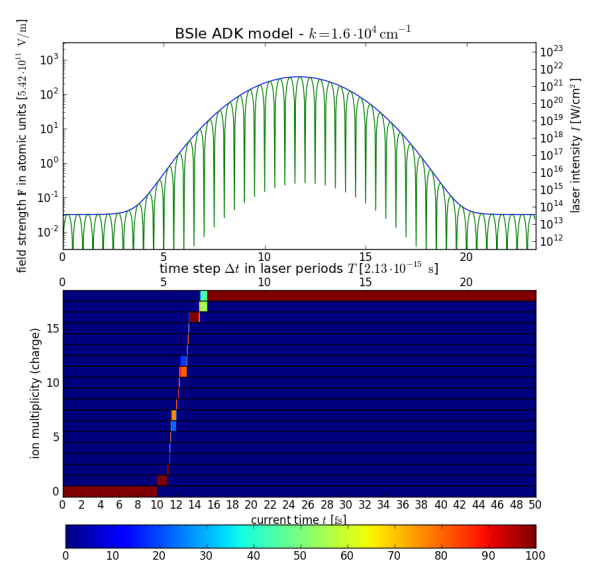


Figure 5.13: BSle ADK model
Wavelength: 640 nm, pulse duration: 50 fs

... The blue curve illustrates the envelope of the pulse.

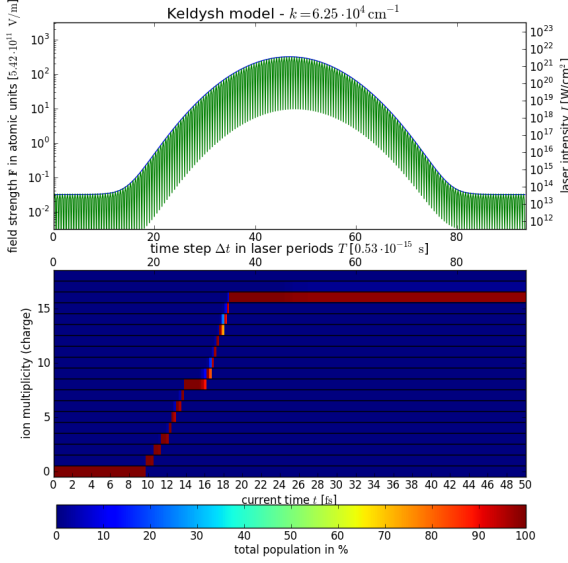


Figure 5.14: Keldysh model
Wavelength: 160 nm, pulse duration: 50 fs

The population of each charge state in percent ...

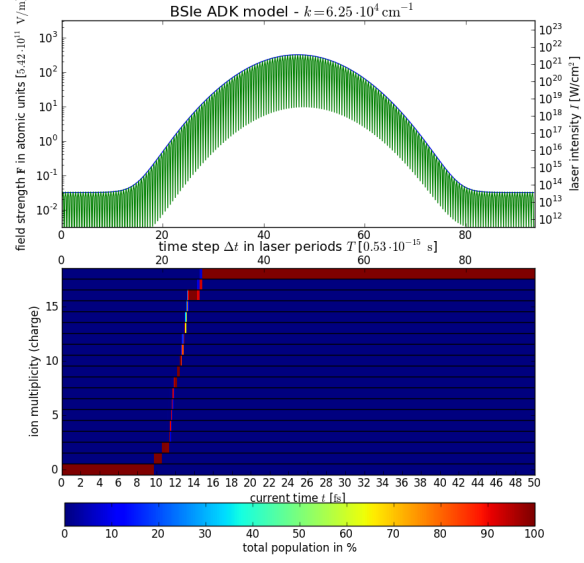


Figure 5.15: BSle ADK model
Wavelength: 160 nm, pulse duration: 50 fs

... is indicated by its color.

In figures 5.11, 5.13 and 5.15 a similar scenario has been simulated, using the BSI-extended ADK model. Again the first, the middle and the last of the wave numbers from table 5.2 are employed and in comparison to the Keldysh model, the ionization happens much more immediate. The times of high population for each charge state have in general become shorter and as such the influence of the different wave numbers is smaller. Mixed charge states can only be seen in figure 5.13 but this seems more related to the time-distributed peaks of the field amplitude coinciding with the small regions of field strength where in this model ionization is noticeable. Thus 20 % or 30 % of the particles are ionized before the amplitude drops, leaving the ratio of populated charge states constant for half a cycle. In contrast to the Keldysh model where the full ionization process took an overall time of about 10 fs, in the BSI-extended ADK model it was already completed in about 4 fs. All three figures for each model share again that the final charge state is reached at the same time with respect to the pulse maximum in the order of femtoseconds.

Interpretation Since the process of interest is field ionization in the tunneling or barrier-suppression regime, the photon energy going along with the wave number is of no importance. However for shorter pulses the wave number k determines the power of the pulse, accounting for a difference in the intensity if energy conservation was to be considered. Ionization processes take energy from the pulse and therefore diminish its intensity. Note that the power of an

envelope-only pulse is double the power of an oscillating field of the same shape, as was shown in chapter 3. However, as energy conservation is neglected still an effect on the ionization dynamics could be perceived. For pulse durations longer than several 10 or 100 femtoseconds wherein many laser cycles are performed, different wave numbers affect the distribution of charge states on time scales of the order of ~ 100 attoseconds to several \sim fs. In the case where the oscillating field has a monotonously growing envelope, charge state population ratios can stay constant for up to half a laser cycle. This could be well perceived in fig. 5.13. If the wave number becomes even higher the delay effect described before vanishes and the ionization dynamics resemble the envelope-only case. It should be remembered, however, that higher wave numbers lead to the multi-photon regime eventually.

Relating the time scales from this analysis to length scales in a simulation yields

$$s = c \frac{T}{2} \approx 3 \cdot 10^8 \frac{\text{m}}{\text{s}} \cdot \frac{30 \text{ fs}}{2} = 4.5 \mu\text{m}. \quad (5.11)$$

Here, T denotes approximately the time where the pulse intensity is varying. In a PIC simulation with similar properties 8 orders of magnitude of intensity would be traversed on a length scale of $4.5 \mu\text{m}$. However this accounts only for the slowly-varying envelope. The oscillation of the field results in intensity gradients of 8 orders of magnitude on sub micrometer scales. Employing different models and wave numbers leads already to very different ionization dynamics in these simulations. Nevertheless such gradients are still moderate compared to the gradients produced in a laser-matter interaction with a solid state target. According to the high electron density of these targets the laser would penetrate only on the $\gtrsim 10 \text{ nm}$ scale. There, the relativistic intensities of $10^{18} \dots 10^{20} \text{ W/cm}^2$ are reduced exponentially to 0. The outcome of simulations with different ionization models might exhibit crucial differences.

5.6 Initial phases in ultrashort pulses

The production of shorter and more intense pulses must currently employ short laser wavelengths [22] in the X-ray regime. Very short pulse durations indicate that the initial phase of the laser wave might have an essential effect on the charge state evolution. The initial phase φ_{initial} determines the regions of low amplitude in space and time. Hence it is expected to have a similar effect as the wave number k . It was observed before, that in a scenario where the pulse duration T_{pulse} large compared to the laser period, mixed charge states were generated. In figures 5.16, 5.18 and 5.20 a much shorter pulse duration of 5 fs has been chosen and the maximum field strength has been reduced to $10^{1.5} \text{ AU}$. The laser wavelength measures $1 \mu\text{m}$ accounting for a laser period of 3.3 fs. It has been sampled with 50 points allowing for no more than roughly one laser cycle under the Gaussian envelope. The initial phases considered are 45° , 60° and 75° . For this set of three simulations in the Keldysh model the particles reach

a maximum charge state of +7. However as the initial phase determines the position of the roots in the $|\sin(\omega t + \varphi_{\text{initial}})|$ -function, varying the field amplitude which results in not only changing the time-dependent succession of charge states but also the final distribution. In figure 5.16 the final state is an ensemble of both +6 and +7 charge states. Except from this figure the final state in the remaining two cases is reached at nearly the same time of about 0.7 laser cycles. The vicinity of a field strength minimum results in a time period of constant charge state population.

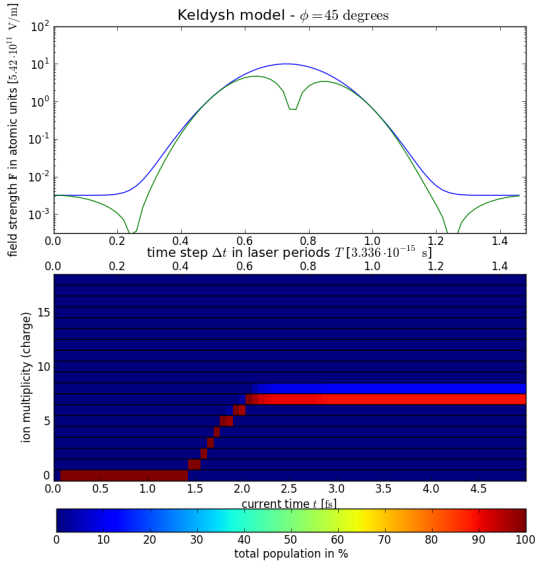


Figure 5.16: Keldysh model
Pulse duration: 5 fs, initial phase: 45°

Charge state evolution for $N = 1000$ particles in a Monte-Carlo simulation. ...

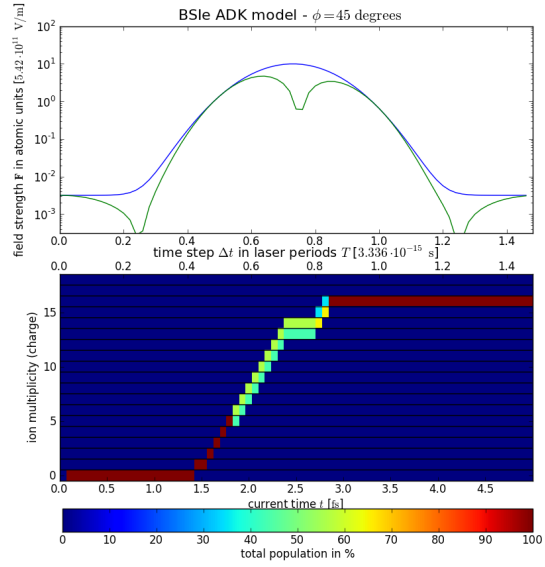


Figure 5.17: BSle ADK model
Pulse duration: 5 fs, initial phase: 45°

... The green line in the upper plot marks the field strength at each moment, ...

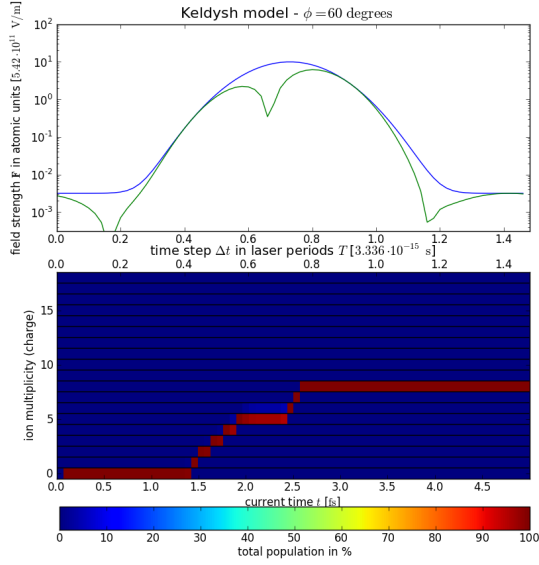


Figure 5.18: Keldysh model
Pulse duration: 5 fs, initial phase: 60°

... from which ionization probabilities were calculated. ...

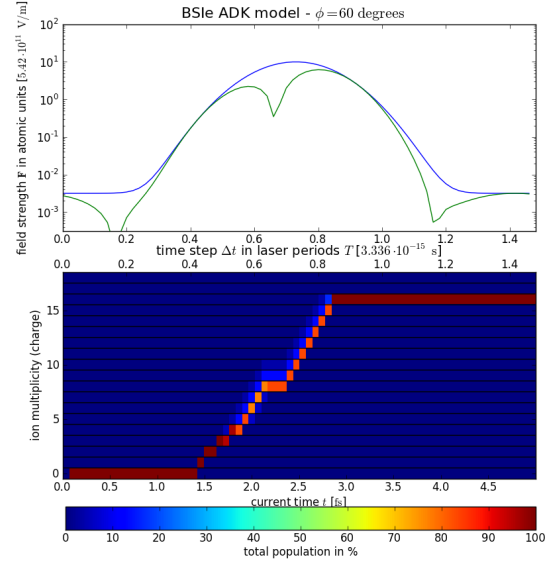


Figure 5.19: BSle ADK model
Pulse duration: 5 fs, initial phase: 60°

... The blue curve illustrates the envelope of the pulse.

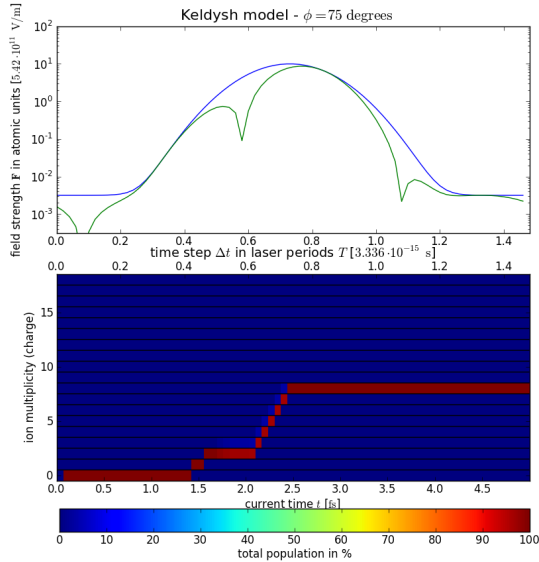


Figure 5.20: Keldysh model
Pulse duration: 5 fs, initial phase: 75°

... The wavelength measures
 $\lambda = 1 \mu\text{m}$

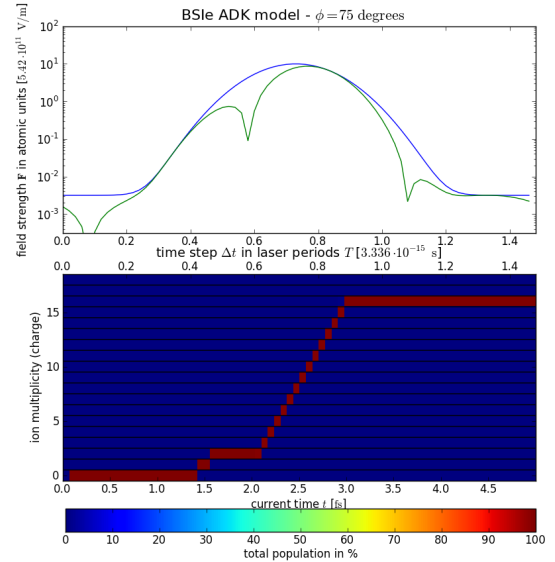


Figure 5.21: BSle ADK model
Pulse duration: 5 fs, initial phase: 75°

... The color in the lower plot indicates the population of the charge state.

The same scenario has been employed in the BSI-extended ADK model. There is a significant difference to the Keldysh model in the final state of the simulations as here the particles

reach +16 multiplicity for each initial phase. Common to the simulations is that the final charge state is reached after about 0.8 laser periods. Different for all three phases φ_{initial} is the sequence of ionization. For an initial phase of 60° in figure 5.19 there exist three subsequent charge states at the same time. Where in fig. 5.21 there is a period of constant charge state +2 only in the beginning, the subsequent states exhibit nearly no visible transition time. In fig. 5.17 starting from the +5 state the lower plot shows that at some time about 55% of the particles get ionized while 45% remain in the lower state. When 0.05 fs these get ionized as well, simultaneously the next higher charge state is populated. The ratio of the two populated states remains constant.

Interpretation In the course of the simulations it has become clear that the final states are reached at the same time independent from the variation of the initial phase. The only exception is when the phase shifts the minimum of the field amplitude to the position where the envelope would reach its maximum. Thus the overall maximum field strength is lower which could result in a lower final charge state. All images share the immediate transitions for large gradients in the vicinity of amplitude minima. In cases where the gradient is not so steep or the peak amplitude of a laser cycle coincides shortly with the tunneling regime of a particular charge state, mixed charge state populations can be generated. On few femtosecond time scales the initial phase φ_{initial} is therefore confirmed to have a similar effect as the wave number k . It is however much more prominent and the differences are more obvious on time scales where $T_{\text{pulse}} \gtrsim T_{\text{period}}$. It is noteworthy that the ratio of the participating charge states stays rather constant in the further increase of the electric field but its actual value can differ much from small changes in the initial phase. In such a way the ionization dynamics can be very different. In a similar fashion to sec 5.5 the results relate to spatial dimensions in a PIC simulation. On a length scale of $0.9\,\mu\text{m}$ 6 orders of magnitude in intensity are traversed. Typical targets measure a few micrometers in depth. In the BSIe ADK model 17 different charge states are distributed on this length scale whereas the Keldysh model predicts only 7 subsequent Argon charge states. Depending strongly on the initial phase of the laser wave mixed charge states might exist and spread over the length of a few $\sim 100\,\text{nm}$ each. Their composition is even more sensitive on φ_{initial} . With higher gradients the outcome in relativistic-intensity laser-matter interaction simulations is currently unpredictable and may to great extent depend on the discretization of the laser pulse.

5.7 Spatial charge state distribution

This section concentrates on an analysis of the differences in the charge state distribution in two dimensions. A simple approximation by the BSI condition is compared to the evolution of

charge states over time and space in two the Keldysh and the BSIe ADK model. Figure 5.23 shows the interaction region at the beginning of a Gaussian pulse of $30\text{ }\mu\text{m}$ length and $3\text{ }\mu\text{m}$ width. The intensities at the locations are depicted in W/cm^2 . Three colored plots below show an approximation of the final charge state distribution predicted by the barrier suppression condition (top), the evolution in the Keldysh model (center) and in the BSI-extended ADK model (bottom).

All three charge state distributions share the general sequence and the size of their overall populated areas with neutral atoms at the right upper and lower edges ranging to $+2$ in the center. It can be seen however that in the Keldysh model already areas populated by one charge state exhibit particles of the next higher charge state, occasionally. The overall distribution is yet similar to that of the BSI-condition. In the case of the BSIe ADK model a clear difference for the small left center region of higher intensities exists. The ions carry a charge of $+8$ in this area and the transition region from the $+2$ -zone only measures a few nanometers. Apart from the latter zone where a few $+4$ and $+6$ -states are spread, the number of single higher charged particles scattered over the regions is much smaller than in the Keldysh simulation.

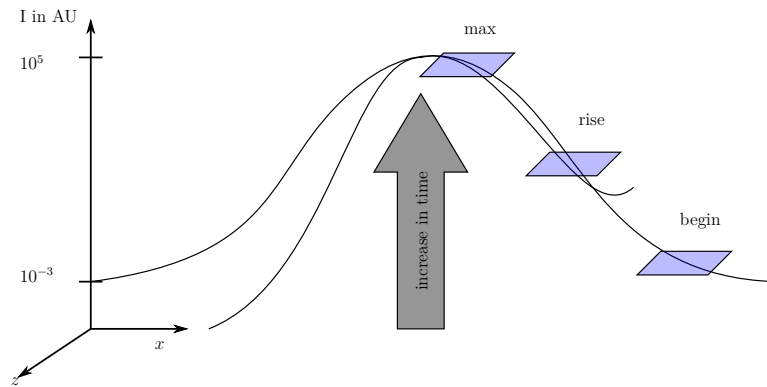
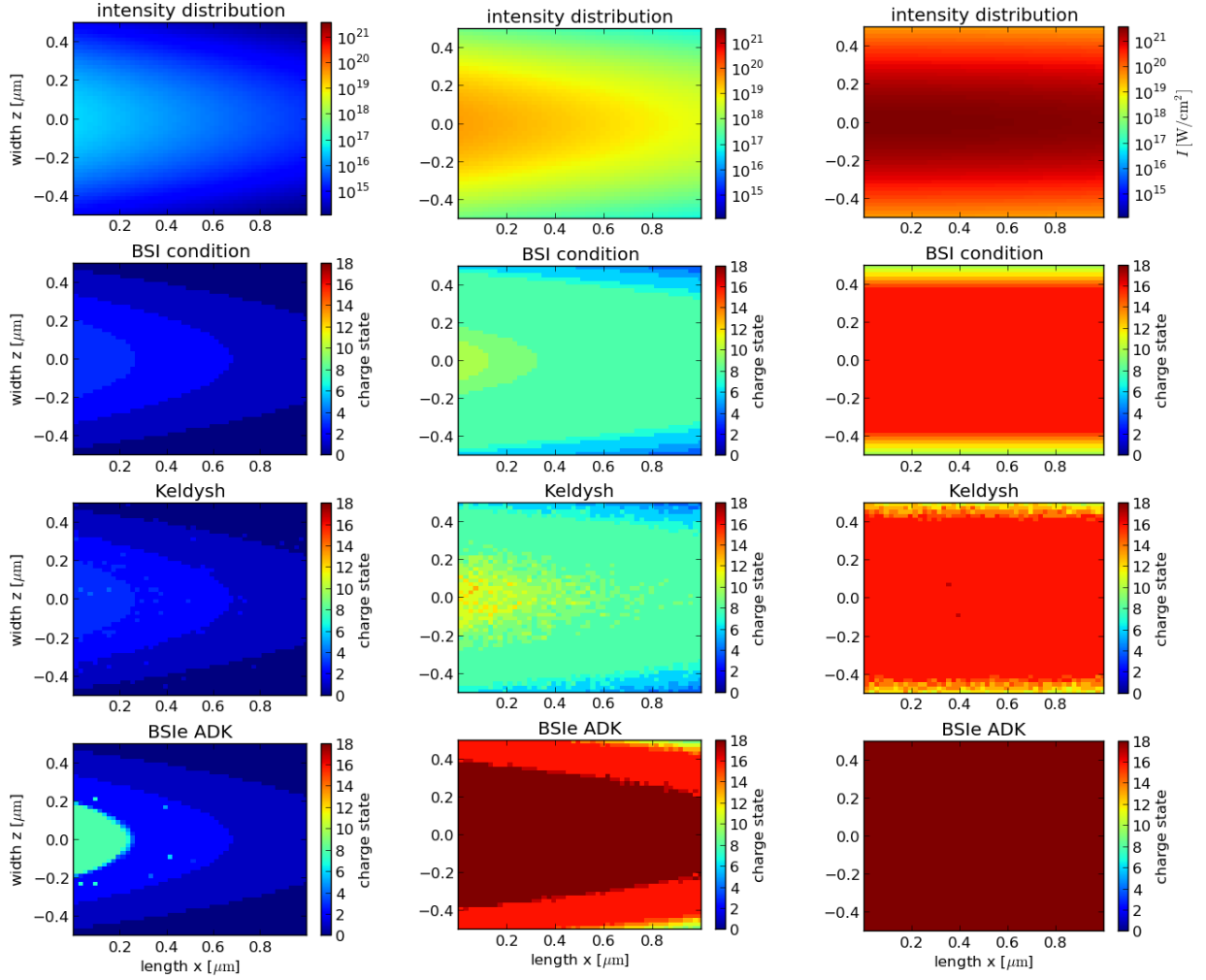


Figure 5.22: Schematic picture of the scenario for the spatio-temporal charge state distribution analysis. The light blue regions mark the regions examined and the values for the intensity I denote the final pulse properties after its linear increase in time for about $T = 6.7\text{ fs}$ and 100 Monte- Carlo iterations

**Figure 5.23:** Low slope region

Spatio-temporal charge state distribution of a Gaussian pulse of $30\mu\text{m}$ length and $3\mu\text{m}$ width interacting with Argon atoms. The upper plot shows the intensity distribution in the region. ...

Figure 5.24: Steep slope region

... The plot below depicts the charge state distribution based on the BSI condition applied to the final pulse shape. The two plots below show the Keldysh model and BSle ADK model results after ...

Figure 5.25: Peak region

... 100 Monte-Carlo iterations in 6.7 fs. The intensities grew linearly from 0 to the distributions shown above. Each image section shows an area of $1\mu\text{m}^2$ from the lateral center of the pulse.

In figure 5.24 the same scenario as before has been simulated in the region of a steeper slope and with laser intensities ranging from about 10^{19} to 10^{20} W/cm^2 on the ridge of the pulse. In lateral direction it ranges from $4 \cdot 10^{17}$ to $8 \cdot 10^{19}\text{ W/cm}^2$. In the BSI approximation the most prominent charge state is +8 and only the small edge areas range down to +4. The highest charge states reached are tenfold positively charged argon ions. The Keldysh simulation shares the large +8-section and also the gradient down to +4. These areas are roughly of the same size of about $0.15\mu\text{m}$ in width at the most. An apparent difference is that in the Keldysh simulation the +9, +10 charge states populate the full length of the target area. Only the width diminishes but in the ridge region near the notional propagating axis they reach up to $0.6\mu\text{m}$ further into the target than predicted by the BSI-condition.

In contrast, the simulation of the BSIE ADK model shows that already at an intensity of about 10^{18} W/cm^2 the +18 charge state is widely populated. On a small, nearly imperceptible area of +17 ions there follows a larger region homogeneously populated by +16 states. It measures about $0.2 \mu\text{m}$ perpendicular to its boundaries. The lowest charge states in this model are +9 in the upper and lower right corners. Figure 5.25 shows the region where on the left side border of the target area, the pulse peak with an intensity of nearly $4 \cdot 10^{21} \text{ W/cm}^2$ is located. The variation of the intensity is far below one order of magnitude and only in z -direction it drops to about $8 \cdot 10^{19} \text{ W/cm}^2$. The barrier suppression condition and the Keldysh model predict a very similar final state with a large, homogeneously distributed area of +16 argon ions and a $0.1 \mu\text{m}$ small transition region down to the +10 state on each side far from the center x -axis. While the barrier suppression condition and the Keldysh model do not predict complete ionization, the BSIE ADK model generates +18 charge states for all of the target region without exception.

Interpretation In the beginning of the pulse in figure 5.23 the prediction by BSI matched the simulated distribution of charges states well, except for the BSIE ADK model. The large areas of homogeneous population it shared with the other two are believed to result from the BSI condition, itself. The previous examinations have shown that for low charge states the BSI-extended ADK model ionizes at higher field strengths than the other models. Since in the Monte-Carlo simulations also the barrier suppression condition is used to prevent unphysical behavior the large areas of +1 and +2 seem likely to have been enforced by it. For higher intensities and subsequently higher charge states the roles of the models quickly exchange which could be seen in fig. 5.24. It is noteworthy how large the differences from the BSI approximation are in this figure. Not only the BSIE ADK model that seems to have very fast ionization dynamics but also the Keldysh model exhibits large regions of higher charge states that were not predicted by barrier suppression. This is of course to be expected since the models describe the tunneling effect which starts to contribute at intensities much lower than the Stark shifted appearance intensity for a charge state. However, it is a fact to be kept in mind when estimating the effect of a laser pulse on a target. Instead of considering the current intensity of a pulse the effect on the target is to be integrated over time. The final state eventually seems to be the same if the peak intensity of the laser is high enough to ionize all atoms and ions completely. During the ionization process however the charge state distributions can differ on micrometer scales, thus altering the ionization dynamics even in underdense target simulations to different results. The extension of the BSI-condition and the Keldysh model to non-hydrogen-like atoms in this thesis may account for the difference in the final states in figure 5.25. However such approximations are commonly used in the application of existing non- relativistic field ionization models to simulation scenarios. It became obvious

in this analysis that these scenarios have to be approached with more care as the existing models yield many problems in the description of the underlying physical processes.

6 Conclusion

The results of this thesis show that in the simulation of laser-matter interaction with existing field ionization models and relativistic intensity, short laser pulses largely different outcomes are produced. Even for moderate gradients where laser intensities vary over 3 to 9 orders of magnitude on the scale of a few femtometers, the ionization dynamics exhibit clearly distinguishable differences. The temporal evolution of a charge state differs on a femtosecond scale depending on the choice of the model. Thus spatio-temporal ionization profiles are different on lengths of ~ 100 nanometers. In current PIC simulations the interaction with solid state targets are simulated. Those simulations feature gradients of up to 21 orders of magnitude over Skin-depth scales of a few ~ 10 nanometers. With such extreme gradients the existing non-relativistic field ionization models cannot be expected to describe the processes accurately, anymore. The extreme conditions of the simulations violate the quasi-static approximations of the models. Smaller time steps would be required to allow for large intensity gradients and to sample a laser wavelength with more than just 50 points. On time scales of a few attoseconds, however, the models cannot be applied either since all of them average over the electron motion. A typical electron orbital cycle measures 150 as. Differences in the prediction of the models grow with the atomic number Z . Thus better extensions to other atoms than hydrogen are required.

7 Outlook

7.1 Outlook

In the course of this thesis energy conservation has been neglected in all simulations. For future analyses an ionization current or the reduction of field strength with each ionization should be introduced. More models and elements could be added to the comparison and an application example could be simulated. Therefore the charge state development for the measured data of a laser pulse produced in the DRACO laser [19] might provide new insight. It is also important to evaluate the error for a PIC simulation using macro-particles. Charge state distributions could be calculated analytically and then be compared to the simulation results. An assessment of a minimum grid size with respect to an error threshold could be gained. In this thesis multi-photon ionization has not been discussed any further than in theory. It is however desirable to evaluate the contribution of this effect to the generation of pre-plasma at the beginning of the laser pulse.

The work of Reiss [15] has provided even stricter limits to the tunneling regime since in the previous theories relativistic effects have been neglected. It could therefore be interesting to evaluate to what extent the existing models leave those boundaries in simulation scenarios. Finally the Z -dependency of the models should be explored further to increase accuracy in the application to a wider range of atoms. The work of [18] can turn out useful for that.

8 Bibliography

- [1] P. Agostini, F. Fabre, G. Mainfray, G. Petite, and N. K. Rahman. Free-Free Transitions Following Six-Photon Ionization of Xenon Atoms. *Physical Review Letters*, 42(17):1127–1130, April 1979.
- [2] M. V. Ammosov, N. B. Delone, and V. P. Krainov. Tunnel ionization of complex atoms and of atomic ions in an alternating electromagnetic field. *Soviet Physics - JETP*, 64(6):1191–1194, 1986.
- [3] D. Bauer and P. Mulser. Exact field ionization rates in the barrier-suppression regime from numerical time-dependent Schrödinger-equation calculations. *Physical Review A*, 59(1):569+, January 1999.
- [4] Berestetskii. Coefficients of spontaneous transitions of hydrogen atom. http://www.ioffe.ru/astro/QC/CMBR/sp_tr.html. Online; 10-June-2013.
- [5] N. B. Delone and Vladimir P. Krainov. Tunneling and barrier-suppression ionization of atoms and ions in a laser radiation field. *Physics-Uspekhi*, 41(5):469–485, May 1998.
- [6] N. B. Delone and Vladimir P. Krainov. AC Stark shift of atomic energy levels. *Physics-Uspekhi*, 42(7):669, 1999.
- [7] F.H.M. Faisal. Exact perturbation theory of multiphoton processes at high intensities. *Il Nuovo Cimento B Series 11*, 33(2):775–795, 1976.
- [8] Hermann Haken and Hans Christoph Wolf. *Atom- und Quantenphysik / Einführung in die experimentellen und theoretischen Grundlagen ; mit 29 Tabellen, 167 Aufgaben und vollständigen Lösungen*. Springer, Berlin ; Heidelberg [u.a.], 6., verb. und erw. Aufl. edition, 1996.
- [9] L. V. Keldysh. Ionization in the field of a strong electromagnetic wave. *Soviet Physics JETP*, 20:1307–1314, May 1965.
- [10] V. P. Krainov. Ionization rates and energy and angular distributions at the barrier-suppression ionization of complex atoms and atomic ions. *J. Opt. Soc. Am. B*, 14(2):425–431, Feb 1997.

-
- [11] L.D. Landau and E.M. Lifshitz. *Course of Theoretical Physics Vol 3 Quantum Mechanics*. Pergamon Press, 1958.
 - [12] Peter Mulser and Dieter Bauer. *High power laser-matter interaction*. Springer tracts in modern physics. Springer, Berlin, 2010.
 - [13] C. Perego, D. Batani, A. Zani, and M. Passoni. Target normal sheath acceleration analytical modeling, comparative study and developments. *Review of Scientific Instruments*, 83(2):02B502, 2012.
 - [14] Vladimir S. Popov. Tunnel and multiphoton ionization of atoms and ions in a strong laser field (Keldysh theory). *Physics-Uspekhi*, 47(9):855–885, October 2007.
 - [15] H. R. Reiss. Limits on Tunneling Theories of Strong-Field Ionization. *Physical Review Letters*, 101(4):043002, July 2008.
 - [16] J. J. Sakurai. *Modern Quantum Mechanics (Revised Edition)*. Addison Wesley, 1 edition, September 1993.
 - [17] H. Schulz. *Statistische Physik: beruhend auf Quantentheorie ; eine Einführung*. Deutsch, 2005.
 - [18] Yulian V. Vanne and Alejandro Saenz. Solution of the time-dependent dirac equation for multiphoton ionization of highly charged hydrogenlike ions. *Phys. Rev. A*, 85:033411, Mar 2012.
 - [19] Rainer Weisflog. Dresden laser acceleration source. <http://www.hzdr.de/db/Cms?p0id=32076&pNid=0>. Online; 10-June-2013.
 - [20] D.M. Wolkow. Über eine klasse von lösungen der diracschen gleichung. *Zeitschrift für Physik*, 94(3-4):250–260, 1935.
 - [21] J.J. Yeh. Atomic calculation of photoionization cross-sections and asymmetry parameters. <http://ulisse.elettra.trieste.it/services/elements/WebElements.html>. Online; 10-June-2013.
 - [22] Song F. Zhao, Xiao X. Zhou, Peng C. Li, and Zhangjin Chen. Isolated short attosecond pulse produced by using an intense few-cycle shaped laser and an ultraviolet attosecond pulse. *Physical Review A (Atomic, Molecular, and Optical Physics)*, 78(6):063404+, December 2008.

Erklärung

Hiermit erkläre ich, dass ich diese Arbeit im Rahmen der Betreuung am Institut für Kern- und Teilchenphysik ohne unzulässige Hilfe Dritter verfasst und alle Quellen als solche gekennzeichnet habe.

Marco Garten
Dresden, Juni 2013